Taylor & Francis
Taylor & Francis Group

REPORT

🔓 OPEN ACCESS | Check for updates

Development and characterization of AD-214, an anti-CXCR4 i-body-Fc fusion for the treatment of idiopathic pulmonary fibrosis

Jason P. Lynch [ID][a], Louise Organ[a], Khamis Tomusange[a], Lukasz Kowalczyk[a], Dallas J. Hartman[a], Angus Tester[a], Chris Hosking[a]*, and Michael Foley [ID][a,b]

[a]AdAlta, LIMS2 Building, Science Drive, La Trobe University, Bundoora, Australia; [b]Department of Biochemistry and Chemistry, La Trobe Institute for Molecular Sciences, La Trobe University, Bundoora, Australia

ABSTRACT

Idiopathic pulmonary fibrosis (IPF) is a chronic, progressive lung disease characterized by scarring and tissue remodeling. Current treatments have limited efficacy and significant side effects. To address these limitations, we developed AD-214, an anti-CXCR4-Fc-fusion protein composed of an anti-CXCR4 i-body (AD-114) tethered at its C terminus to constant domains 2 and 3 of the Fc region of a mutated human IgG1 lacking effector function. AD-214 binds with high affinity and specificity to CXCR4, modulates intracellular signaling, and inhibits key fibrotic pathways. Using fibrosis models, we demonstrate that AD-214 treatment significantly reduces collagen deposition and lung remodeling and has a unique mode of action. In Phase 1 clinical trials, intravenous infusion of AD-214 led to high and sustained CXCR4 receptor occupancy (RO), but whether RO and efficacy are causally linked remained to be determined. Herein, we demonstrate that CXCR4 RO by AD-214 inhibits primary human leukocyte migration, a model fibrotic process, and that migration inhibition is achievable at concentrations of AD-214 present in the serum of healthy human volunteers administered AD-214. Taken together, these data provide proof of concept for AD-214 as a novel treatment strategy for IPF and suggest that clinically feasible dosing regimens may be efficacious.

Introduction

Idiopathic pulmonary fibrosis (IPF) is a type of interstitial lung disease (ILD) characterized by fibrosis or scarring in the lung parenchyma.[1] Life expectancy for IPF patients is typically just 2–5 years post-diagnosis and currently the only cure is a double lung transplant. The first drugs for IPF were approved in the US in 2014 but have limited effect: they slow (but do not halt) progression, confer approximately an additional year of life expectancy, and have serious side effects resulting in 30–50% of patients discontinuing therapy within a year.[2] Although drugs for IPF have been evaluated in over 50 Phase 2 and Phase 3 clinical trials in the past 10 years, no new therapeutic agents have been approved since 2014. Thus, there is an unmet need for more effective therapies for IPF.

C-X-C chemokine receptor type 4 (CXCR4), a member of the G protein-coupled receptor (GPCR) superfamily, is expressed on the surface of various cell types, including immune cells and stem cells. The binding of the chemokine ligand CXCL12/SDF-1 to CXCR4 activates intracellular signaling pathways that regulate the movement of cells toward the source of the chemokine.[3–5] This chemotactic response is used by immune cells, such as T cells and monocytes, to navigate from the bloodstream to tissues and for these cells to reach sites of infection or injury. Additionally, CXCR4 is involved in the migration of hematopoietic stem cells, including the maintenance of white blood cell populations in the bone marrow and their mobilization into the bloodstream.[6] Beyond its normal physiological role, CXCR4 has been implicated in various pathological conditions such as HIV infection, cancer metastasis, and fibrosis occurring in various organs, including the lungs. In patients with IPF, the expression of both CXCR4 and CXCL12 is increased[7–10] while a reduction in CXCR4 expression over time was associated with better outcomes in IPF patients.[9] Blockade of CXCR4 using the small-molecule inhibitor AMD3100 (plerixafor) has demonstrated efficacy in preclinical models,[8,11–13] but its rapid clearance from the circulation and potential cardiotoxic effects limit its utility for IPF treatment where chronic administration is necessary. Anti-CXCR4 antibodies have been developed to increase the specificity and hence reduce the potential for off target effects often seen with small molecules. However, as these antibodies harbor a fully functional Fc domain, they can induce antibody-dependent cellular cytotoxicity (ADCC) and complement-dependent cytotoxicity (CDC)[14,15] or induce a reduction in cell proliferation due to apoptosis,[16,17] which would be desirable for their cancer cell killing properties, but could be detrimental in the context of fibrotic diseases. Thus, developing new targeted therapies whose specific function is to block CXCR4 signaling and prevent downstream function has

become an important area of research for the treatment of fibrotic diseases.

We previously developed AD-114, a fully human single-domain i-body that specifically binds human CXCR4 with nanomolar affinity and is effective at inhibiting a number of CXCR4-mediated functional activities *in vitro* and *in vivo* that lead to the progression of IPF.[13,18] Being a single-domain i-body, AD-114 has a short circulatory half-life, although several approaches have been used to improve this.[19] Here, we describe the development of a second-generation molecule, AD-214, which consists of the i-body AD-114 fused to an Fc moiety from an IgG1 that has been mutated to silence its effector functions. AD-214 exhibits enhanced avidity, extended half-life, and improved manufacturability. We also show that AD-214 binding to CXCR4 can modulate intracellular signaling and block the progression of fibrosis in *ex vivo* human tissues, as well as a bleomycin-induced mouse model of fibrosis.

Results

Construction and characterisation of AD-214

Initial experiments examined the fusion of AD-114 with the Fc region of both native IgG1 and IgG2 with different linkers and with different signal peptides (Figure S1a). Inclusion of a functional Fc domain would initiate effector responses leading to immune cell killing and inflammation, which would be detrimental in the context of fibrosis;

therefore, we chose the IgG1 DAPA mutant as the fusion partner for AD-114 to modulate its ability to induce FcγR-based effector functions (see below). This i-body-Fc fusion was termed AD-214 (Figure 1a and Figure S1b). Under reducing and non-reducing SDS-PAGE analysis, the protein migrated at the expected molecular weights of approximately 37.5 and 75 kDa, respectively, for the monomeric and dimeric versions of a disulfide-linked Fc fusion protein. AD-214 is predominantly monomeric when assessed by size exclusion chromatography (Figure 1b) and has a ~10 pM binding affinity to CXCR4 when analyzed by surface plasmon resonance (SPR) against human CXCR4 displayed on virus-like particles (Figure 1c). This is an almost 1,000-fold increased affinity to CXCR4 over AD-114 (~4 nM).[18] This improved affinity was consistent with an increased avidity of AD-214 due to the bivalent nature of the Fc fusion. As expected, the IgG1 DAPA Fc moiety was found to interact with human FcRn with an affinity of ~48 nM (Figure 1d), similar to published affinities for wild type Fc.[20] The binding specificity of AD-214 to CXCR4 was investigated using a Membrane Proteome Array platform (Integral Molecular), which detects binding to 5,300 human membrane proteins and can be used to determine target specificity since all target proteins have native conformations and appropriate post-translational modifications. When AD-214 was tested for reactivity in this assay, only cells expressing CXCR4 were detected (Figure 1e); thus, AD-214 retains exquisite specificity for its target.
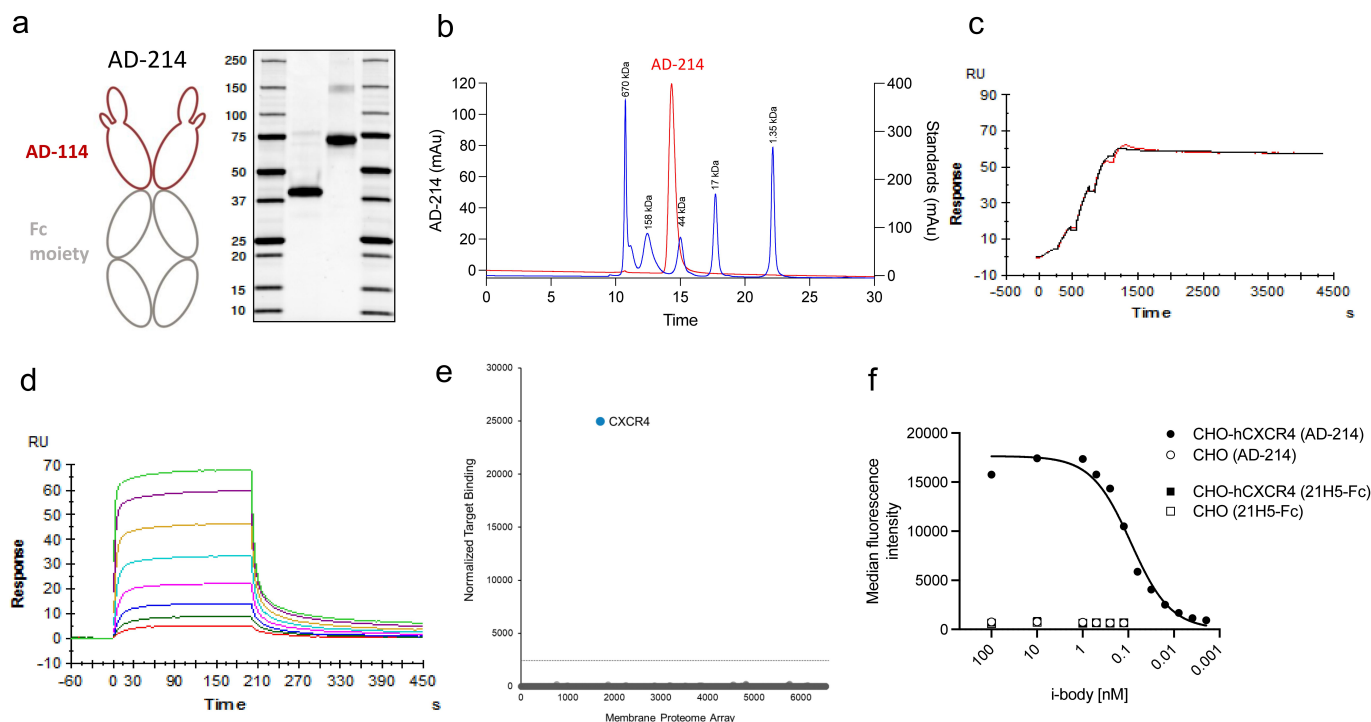

Figure 1. Construction and characterisation of AD-214. (a) Schematic of AD-214 (left panel). Two molecules of anti-CXCR4 i-body AD-114 (red) fused to an Fc moiety harbouring the DAPA mutation to remove effector function (grey). Western blot of purified AD-214 reduced (left lane) and non-reduced (right lane) probed with anti-Fc antibody (right panel). (b) Chromatogram of AD-214 analysed by size exclusion chromatography (SEC). The retention time for AD-214 was 14.303 min. (c) Sensorgram of AD-214 binding to immobilized human CXCR4. Injected concentrations were 0–20 nM. Binding responses (red line) are overlaid with fit of a simple 1:1 kinetic interaction model (black lines). (d) Sensorgram of human FcRn binding to AD214. Injected concentrations were 0–250 nM. Sensorgrams are shown as coloured lines. (e) AD-214 was screened for specificity using integral molecular's membrane proteome array, consisting of ~5,300 human membrane proteins in their native state in unfixed cells. Antibody binding was detected by flow cytometry, and hits were defined as a binding signal more than 3 standard deviations higher than background and validated in follow-up assays. Unlabelled black dots represent hits that were below the defined threshold or that did not validate on retesting. (f) AD-214 binding to human (h)CXCR4 expressed on CHO cells. Bound AD-214 was detected using fluorescently conjugated anti-Fc antibody. MFI, median fluorescence intensity.

Next, we determined the affinity of AD-214 for human (h) CXCR4 on cells. Binding assays were conducted by incubating a concentration gradient of AD-214 (100 nM–<0.1 nM) with a Chinese hamster ovary (CHO) cell line engineered for inducible overexpression of CXCR4 on their surface. We found that AD-214 binds to hCXCR4 on CHO cells with an estimated K_D of 107.1 pM (Figure 1f). No binding to the parental empty vector control CHO line was detected and CHO-hCXCR4 cells treated with control i-body, 21H5-Fc (DAPA), showed no binding, demonstrating that binding of AD-214 to hCXCR4 was specific. In a cell line expressing (~5-fold) lower levels of CXCR4 (U266, Figure S2a), AD-214's affinity was similarly high (K_D: 115 pM) (Figure S2b). Although AD-214 binding to CXCR4 expressed on cells is slightly lower than the binding to CXCR4 on virus-like particles as measured by SPR, the affinity is nevertheless very high and clinically relevant.

AD-214 modulates CXCR4 intracellular signalling

We next examined whether AD-214 could affect the downstream signaling of CXCR4 in response to its ligand CXCL12. CXCL12 binding to CXCR4 induces intracellular signaling via ß-arrestin recruitment and a reduction in cAMP levels that can ultimately lead to cell proliferation and migration. In addition, ligand binding can lead to receptor internalization, via an endocytic pathway. Therefore, we examined the effect of AD-214 on CXCL12 activation of β-arrestin, cAMP, as well as receptor internalization (Figure 2a–e). The ability of AD-214 to antagonize CXCL12-mediated internalization of CXCR4, recruitment of β-arrestin, and downregulation of cAMP was investigated in HEK293FT cells transiently expressing human CXCR4. CXCL12 exhibited a 50% effective concentration (EC_{50}) of 1.7 nM for β-arrestin recruitment, 2.1 nM for cAMP reduction, and 68 nM for CXCR4 internalization,

respectively. This signaling was inhibited by AD-214 with IC_{50} values of 7.1, 8.8, and 7.3 nM for β-arrestin recruitment, cAMP reduction, and CXCR4 internalization, respectively (Figure 2a–d). We also found that AD-214 could block CXCL12-induced calcium influx with an IC_{50} of 56 nM (Figure 2e). These values are significantly more potent than previously reported for the i-body AD-114 without the Fc moiety (Ref. 18,19; Figure 2a) and were also more potent than for the small-molecule CXCR4 antagonist AMD3465 described in the literature (Figure 2a). Thus, AD-214 modulates β-arrestin recruitment, cAMP reduction, and CXCR4 internalization at low nanomolar concentrations but requires 10-fold more protein to inhibit calcium influx, consistent with the previous reports of AD-114 being less potent in modulating CXCL12-induced calcium influx.[18]

AD-214 does not activate ADCC, CDC, or ADCP but has an extended half-life in non-human primates

As noted, in the design of AD-214, we selected an IgG1 with two point mutations (DAPA) as the fusion partner for AD-114 (Figure S3), which has been reported to abolish interactions with the Fcγ receptors that are responsible for mediating effector functions.[21] We confirmed that AD-214 lacks effector functions, specifically ADCC, CDC, and antibody-dependent cellular phagocytosis (ADCP) using in vitro assays (Figure 3a–c). These reporter assays used Ramos cells as target cells and reporter cell lines engineered to express human FcγRIIa as effector cells. Antibodies that have been reported to exhibit effector functions, Rituxan (anti-CD20) and Darzalex (anti-CD38), were used as positive controls and conferred the expected responses in these assays.

Next, the pharmacokinetics (PK) of intravenous (IV) administration of AD-214 (10, 30, and 100 mg/kg) was

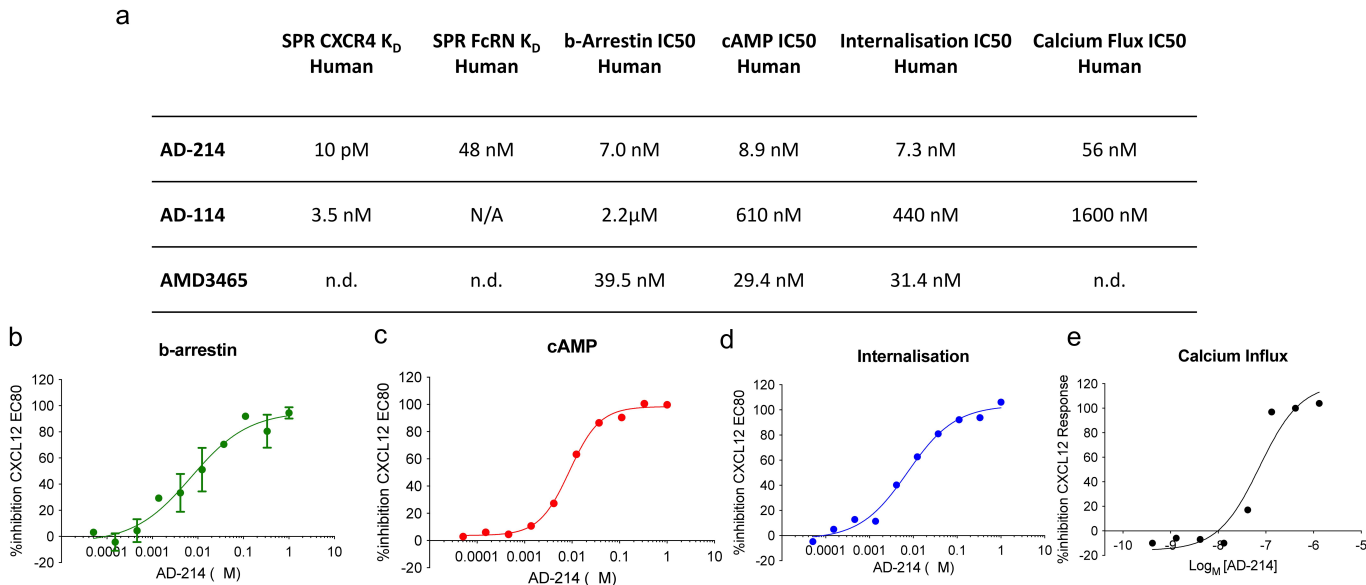|	SPR CXCR4 K_D Human	SPR FcRN K_D Human	b-Arrestin IC50 Human	cAMP IC50 Human	Internalisation IC50 Human	Calcium Flux IC50 Human
AD-214	10 pM	48 nM	7.0 nM	8.9 nM	7.3 nM	56 nM
AD-114	3.5 nM	N/A	2.2 μM	610 nM	440 nM	1600 nM
AMD3465	n.d.	n.d.	39.5 nM	29.4 nM	31.4 nM	n.d.

Figure 2. Pharmacological characterization of AD-214. (a) Table summarizing pharmacological characterization of AD-214. (b–e) AD-214 was tested in antagonist mode with the following DiscoverX biosensor assays: b-arrestin (b), cAMP (c), internalization (total) (d), and calcium flux (e). Data were normalized to the maximal and minimal response observed in the presence of EC80 ligand and vehicle and fit to a non-linear regression curve from which the IC50 was calculated. For Gi cAMP assays, a forskolin concentration of 20 μM was used. Data presented as % inhibition, with average of buffer wells set as 100% inhibition and the average of control agonist EC80 wells set as 0% inhibition.
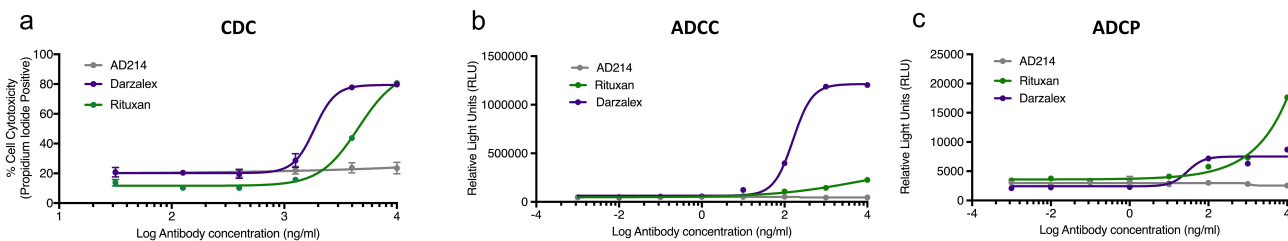
Figure 3. AD-214 lacks effector function. (a) CDC, (b) ADCC, and (c) ADCP assays. For ADCC and ADCP assays, Ramos cells were used as target cells and reporter cell lines engineered to express human FcγRIIa were used as effector cells. For ADCC and ADCP assays, a fixed effector to target ratio of 5:1 was used and AD-214, Rituxan, or Darzalex were evaluated with top concentration of 10 μg/mL followed by a log dilution series (7 points) in triplicate for 6 h at 37℃. Data are plotted as RLU (relative luminescence units) against the log of the test article concentration. For CDC assays, Ramos cells were treated with a semi-log dilution series starting at 100 μg/ml followed by a (7 points) of AD-214, Rituxan, or Darzalex in triplicate with a final concentration of 25% normal human serum complement. Data are plotted as percentage PI against the log of the test article concentration.

evaluated in a repeat dose study in cynomolgus monkeys (*Macaca fascicularis*). As shown in Table S1, AD-214 or control (vehicle diluent) was administered to groups of monkeys twice weekly by IV infusion for four consecutive weeks (Days 1, 4, 8, 11, 15, 18, 22, and 25), and AD-214 was measured in serum pre-dose and over a time course (15 min–72 h) following Day 1 and 25 post-drug administration. AD-214 was undetectable in vehicle control-treated animals (Group 1). In all treated groups (Groups 2–4), as shown in Table S1 and Figure S4a-b, the maximum serum concentration (Cmax) of AD-214 at each dose was reached 15 min post-start of infusion. As shown in Table 1, after Tmax (time to maximum drug concentration), the AD-214 serum concentrations declined at estimated $t_{1/2}$ values ranging from 8.83 to 61.5 h. Clearance (Cl) rates varied from 20.9 to 67.1 mL/h/kg on Days 1 and 25. The estimated t½ was on average 22–29 h and consistent with rapid, saturable target-mediated clearance, followed by slower terminal clearance phase (Table 1 and Figure S4a-b). The volumes of distribution (Vz) ranged from 694 to 3280 mL/kg on both occasions (Table 1). Over the entire dose range, the animals' exposure to AD-214 (based on AUC0-T$_{last}$: area under the serum drug concentration–time curve from the time of dosing to the last quantifiable concentration; AUC∞: area under the serum drug concentration–time curve from the time of dosing extrapolated to infinity and Cmax values) on Days 1 and 25 increased dose-dependently and in a more than dose-proportional manner (Table 1). Finally, Cmax and AUC accumulation ratio (the ratio of accumulation of a drug after

repeated administration as compared to single dose) suggested that AD-214 did not accumulate when administered twice weekly for 4 weeks by IV infusion over 15 min at doses up to 100 mg/kg and that AD-214 was available for >3 days. In addition, there were no clinical signs of overt toxicity that could be attributed to the administration of AD-214 following doses up to 100 mg/kg (human equivalent dose of 30 mg/kg).

AD-214 modulates markers of fibrosis and inflammation

To gain insight into the consequences of blocking CXCR4 signaling with AD-214 in a fibrotic disease setting, we used the BioMAP® Fibrosis Panel.[22,23] In this system, a panel of three primary non-diseased human co-cultured cell types relevant for fibrosis are exposed to transforming growth factor-ß (TGFβ) and tumor necrosis factor (TNF) to model myofibroblast differentiation during chronic inflammation and wound healing in different tissue settings. This system consists of a co-culture of lung fibroblasts alone or with lung epithelial cells, and another co-culture of lung fibroblasts with renal epithelial cells. Information on the phenotype produced by incubating AD-214 at a range of concentrations of potential clinical relevance was evaluated in these systems by measuring an array of disease-relevant protein biomarkers (Figure 4). These studies revealed that AD-214 is not cytotoxic at the concentrations tested as determined by measuring the total protein content of the test wells using the binding of sulforhodamine B (SRB) to cellular proteins (SRB marker in Figure 4, *p*

Table 1. Pharmacokinetic analysis of AD-214 in non-human primates.

Group	Dose (mg/kg)	Sex	Cmax (μg/mL) ± SE	AUC0-Tlast h*μg/mL ± SE	AUC∞ h*μg/mL	t½ (h)	Cl (mL/h/kg)	Vz (mL/kg)
Day 1								
2	10	M	243 ± 21.1	228 ±17.7	228 ± 17.7	24 ± 1.0	44.3 ± 3.6	1540 ± 186
		F	212 ± 27.1	171 ± 30	171 ± 30	22.7 ± 0.8	63.1 ± 13.4	2060 ± 436
3	30	M	583 ± 6.44	1010 ± 75.4	1010 ± 76.6	25.9 ± 1.9	30 ± 2.4	1120 ± 112
		F	541 ± 11.4	703 ± 60.3	707 ± 60.2	28.6 ± 1.2	43.1 ± 3.9	1760 ± 81.5
4	100	M	1770 ± 79.7	4840 ± 383	4850 ± 383	25.7 ± 1.5	21.1 ± 1.4	787 ± 81.2
		F	1640 ± 140	4610 ± 248	4620 ± 249	21.8 ± 1.5	21.9 ± 1.2	694 ± 76.6
Day 25								
2	10	M	174 ± 15.3	187 ± 5.58	193 ± 0.8	35 ± 22.4	51.8 ± 0.2	2610 ± 1670
		F	192 ± 45.7	160 ± 30.3	160 ± 30. 1	8.83 ± 3.1	67.1 ± 12.7	770 ± 255
3	30	M	642 ± 45.6	1170 ± 168	1180 ± 167	*35.7 ± 14.2	26.6 ± 4.3	1490 ± 705
		F	667 ± 27	781 ± 60.2	804 ± 71.1	61.5 ± 15.2	37.9 ± 3.1	3280 ± 729
4	100	M	1880 ± 113	4660 ± 352	4670 ± 353	29.5 ± 8.6	21.9 ± 1.6	857 ± 192
		F	1780 ± 168	5020 ± 587	5040 ± 587	26.4 ± 6.4	20.9 ± 2.3	856 ± 251

Data are presented as mean ± SE. *R2 adjusted = 0.77 (<0.8). M, male; F, Female. Cmax, peak serum drug concentration; AUC, area underthe plasma concentration time curve; t½, plasma elimination half-life; CL, plasma clearance; Vz, volume of distribution; SE, standarderror.
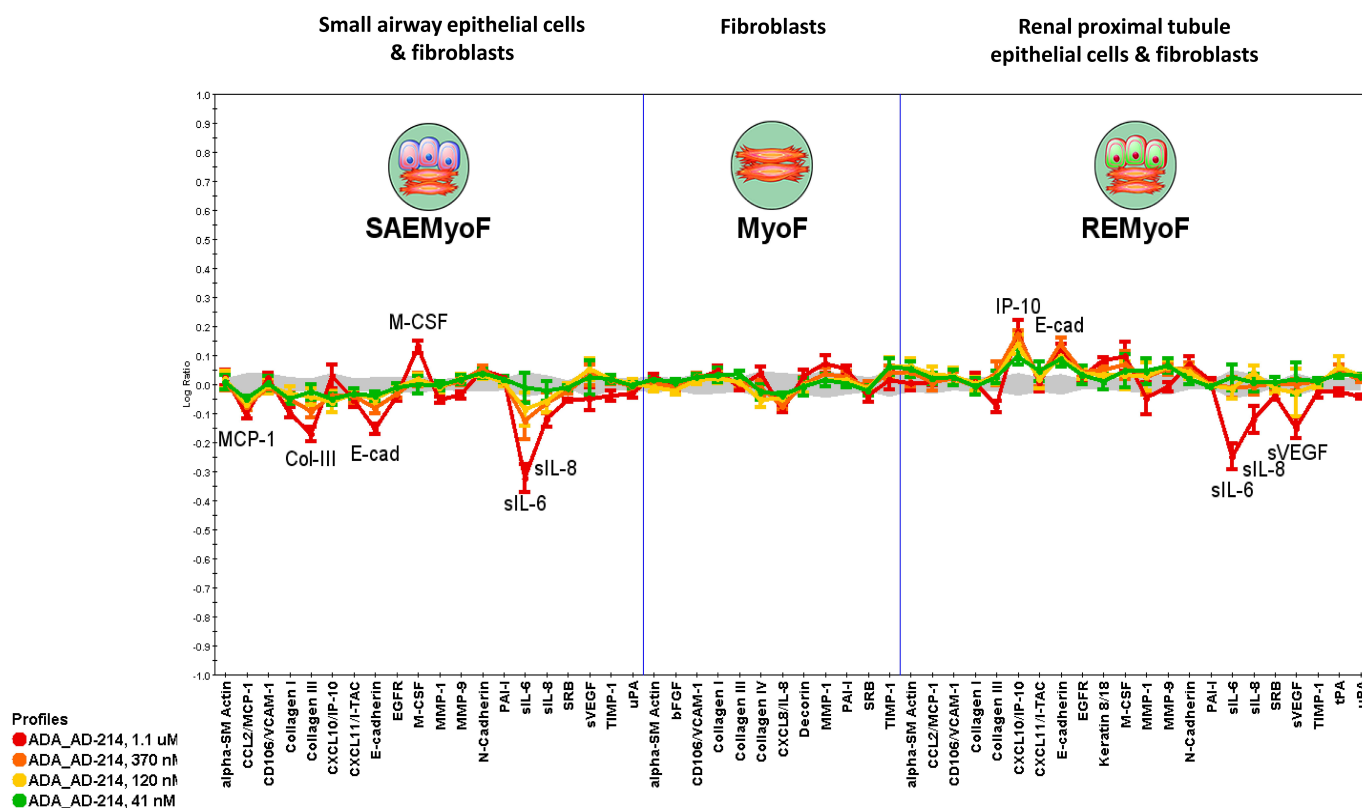
Figure 4. Effect of AD-214 on BioMAP® fibrosis systems. Human primary lung fibroblasts pooled from multiple donors were stimulated for 48 h with a pro-fibrogenic cocktail of TNF and TGFβ are cultured either alone (MyoF) or in co-culture with human small airway epithelial cells (SAEMyoF, modeling lung fibrosis) or human renal proximal tubule epithelial cells (REMyoF, modeling kidney fibrotic disease) and treated with AD-214 (1100, 370, 120, 41 nM). The effects of AD-214 on protein-based readouts in each system (x-axis) are displayed as a log_{10} ratio over vehicle control (y-axis). The gray region around the Y-axis represents the 95% significance envelope generated from historical vehicle controls. A dose-dependent modulation outside of this envelope suggest biological/therapeutic relevance in fibrosis. Line colors indicate different AD-214 test concentrations. Prefix "s" denotes soluble readouts measured in the system supernatant, other readouts are cell-associated. Error bars denote standard error: variation of the raw biomarker measurements from both AD-214 treated samples and vehicle control treated samples.

> 0.05). AD-214 was active in both small airway epithelial cell/differentiated lung myofibroblast co-culture lung (SAEMyoF) and renal (REMyoF) systems and had little activity in the MyoF monoculture system (Figure 4), indicating that AD-214 primarily impacts epithelial cell biology or the paracrine signaling that occurs between epithelial cells and fibroblasts. In the lung system, AD-214 resulted in a decrease of the fibrosis-related matrix markers collagen I and collagen III ($p < 0.01$). In addition, monocyte chemoattractant protein (MCP-1), a chemokine that regulates recruitment of monocytes and T cells into the site of inflammation was significantly reduced. Common activities in both the lung and renal systems included a decrease in sIL-6 ($p < 0.01$) and sIL-8 ($p < 0.01$) expression. Interestingly, AD-214 differentially affected E-cadherin, a marker of epithelial cells that mediates cell–cell contact, in the two systems: expression was decreased in the lung system ($p < 0.01$) and increased in the renal system ($p < 0.01$). Notably, there was no change in the epithelial marker N-cadherin in the SAEMyoF system ($p > 0.05$). Overall, these results suggest that AD-214 could have a role in reducing myofibroblast formation, inflammation, and fibrosis development in the lung and perhaps also the kidney.

Using this system, we next compared the AD-214 response to that of nintedanib and pirfenidone, two therapeutics approved for the treatment of IPF (Figure S5a). Comparing AD-214 and nintedanib (Figure S5a), only one

common activity was annotated within the REMyoF system (reduction of sVEGF) and 14 differentiating activities within the SAEMyoF (MCP-1, E-cadherin, M-CSF, sIL-6, sIL-8), MyoF (VCAM-1, Collagen I, PAI-1, TIMP-1), and REMyoF systems (Collagen I, IP-10, I-TAC, E-cadherin, MMP-9). Comparing AD-214 to pirfenidone (Figure S5b), again there was one common activity reduced in the SAEMyoF system, Collagen III, but only seven differentiating activities were observed within the SAEMyoF (M-CSF), MyoF (Collagen I, Collagen IV, PAI-1), and REMyoF systems (MCP-1, E-cadherin, sVEGF). Overall, these data demonstrate that AD-214 has a different signaling profile to pirfenidone and nintedanib.

AD-214 reduces collagen deposition in human lung

Precision-cut lung slices (PCLS) provide an *ex-vivo* model that has the potential to indicate the translational relevance of a given therapy for lung fibrosis.[24] Fibrogenesis can be induced in PCLS from healthy lungs using a fibrotic cocktail of cytokines and growth factors that drive pulmonary fibrosis and mimic those seen in IPF, including increased extracellular matrix (ECM) deposition and alveolar remodeling. This fibrosis model can be used to assess anti-fibrotic and other properties of novel compounds.[25-27] PCLS from three donors (Figure S6) were cultured *in vitro*

in control media or media with a fibrotic cocktail consisting of TGF-β, platelet-derived growth factor-AB (PDGF-AB), TNF, and lysophosphatidic acid (LPA). Culture media minus the fibrotic cocktail resulted in no deposition of collagen as assessed by Masson's trichrome staining (Figure 5a top left). The fibrotic cocktail induced a significant increase in collagen deposition (Figure 5a top middle and Figure 5b). To assess the effects of AD-214 on collagen deposition, PCLS were stimulated with fibrotic cocktail for 48 h, known to be sufficient to induce early fibrotic like changes,[28,29] before the addition of AD-214, control i-body, 21H5-Fc (DAPA), or nintedanib for an additional 72 h. PCLS treated with the control i-body 21H5-Fc showed a similar increase in collagen as treatment with the fibrotic cocktail (Figure 5a top right). In contrast, treatment with AD-214 resulted in a significantly reduced level of collagen (Figure 5a bottom left and Figure 5b). Although there was a trend for lower levels of collagen in response to nintedanib treatment, this was not statistically significant (Figure 5a bottom right and Figure 5b). These data indicate that AD-214 can induce a reduction in collagen in human lung in response to fibrotic stimuli.

Murine bleomycin model of lung injury

Bleomycin models have been used extensively to model human lung fibrosis and to test for preclinical efficacy of molecules with antifibrotic activity.[30,31] A bleomycin mouse model was therefore used to determine the pre-clinical efficacy of AD-214 in modulating pulmonary fibrosis *in vivo*. Mice were treated with AD-214 starting at day 8 after bleomycin administration, at which point dosing began with pirfenidone (30 mg/kg) and nintedanib (60 mg/kg) until day 21. AD-214 and the control i-body 21H5-Fc (DAPA) (30 mg/kg) were administered every 2 days at 0.01, 1, 10, or 30 mg/kg or every 4 days at 10 and 30 mg/kg. Bleomycin administration induced lung remodeling as early as day 8 (shown as a dotted line in Figure 6) and apparent remodeling after 21 days was evident by histological Ashcroft

scoring of groups treated with bleomycin alone (second bar in Figure 6). Administration of AD-214 at 1, 10, or 30 mg/kg every 2 days from day 8 to day 21 markedly ameliorated fibrotic lung remodeling relative to vehicle control, as assessed by Ashcroft Scoring (Figure 6). At 21 days, the group treated with AD-214 at the lowest concentration of 0.01 mg/kg did not show a significant effect on fibrosis as it was indistinguishable from the group treated with bleomycin alone. In contrast, AD-214 groups treated with 10 mg/kg or 30 mg/kg every 4 days showed a significant decline in Ashcroft scores at day 21 (Figure 6), suggesting that the progression of lung fibrosis was reduced after the commencement of AD-214 treatment. Treatment with pirfenidone and nintedanib at the concentrations indicated did not result in a significant reduction of Ashcroft scores in this model (Figure 6). These results suggest that targeting CXCR4 signaling via AD-214 effectively ameliorated fibrotic lung remodeling in a preclinical murine model of lung fibrosis.

Linking CXCR4 receptor occupancy with efficacy for AD-214

We next sought to develop a method to determine doses of AD-214 that would be potentially efficacious in Phase 2 clinical trials. Unpublished results from a Phase 1 trial of AD-214 trial of AD-214 (NCT04415671) revealed high and durable CXCR4 receptor occupancy (RO) by AD-214 on circulating T cells. To determine whether RO is sufficient to inhibit a model fibrotic process, we developed an *ex vivo* model system whereby RO and a measure of efficacy, T cell migration, can be causally linked. To mimic the *in vivo* situation, we elected to use primary human T cells isolated from cryopreserved buffy coat samples obtained from non-diseased donors, the sampling method, and demographics for which have been reported previously.[7] Notably, these cells are age-matched to IPF patients (>50 years). We first carried out characterization of the buffy coats. First, we demonstrated that the CD3+ lymphocyte population are predominantly T cells (65% CD4+ and 33% CD8+) (Figure S7a) and express CXCR4
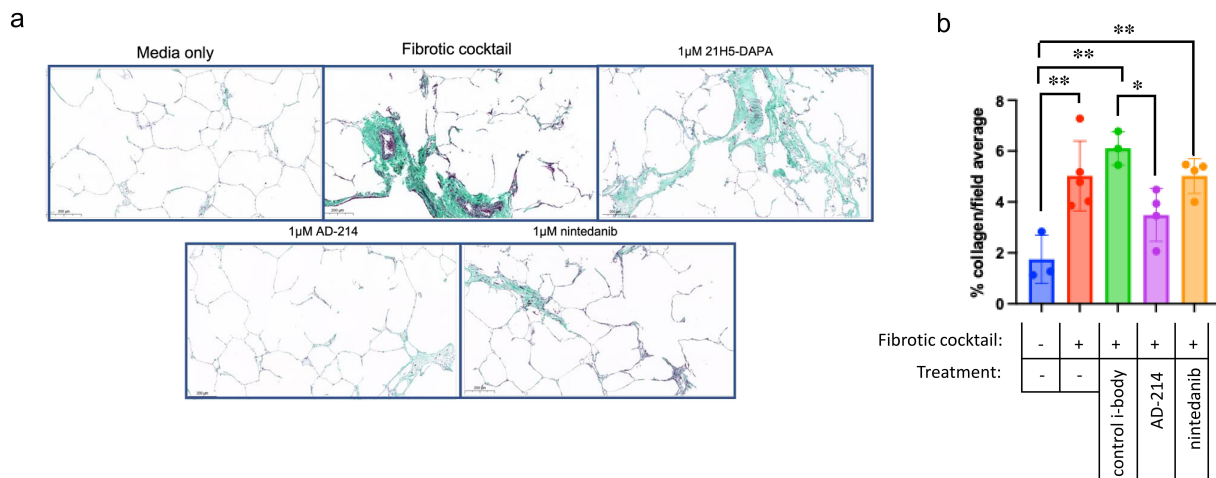

Figure 5. Effect of AD-214 in a PCLS fibrosis model. Human PCLS were exposed to a fibrotic cocktail for 48 h with or without 1 µM of treatment as indicated. Representative images are shown in (a). The area of collagen was measured in sections of human lung slices stained with Masson's trichrome stain; the area of collagen/total field of lung tissue, measured in 10 fields/section to give an average % for each section (b). Each data point represents an individual lung slice. Data is presented a mean ± standard deviation. One-way ANOVA, *<0.05, **<0.01, n = 3–5 donors, 1–2 sections/donor/condition.
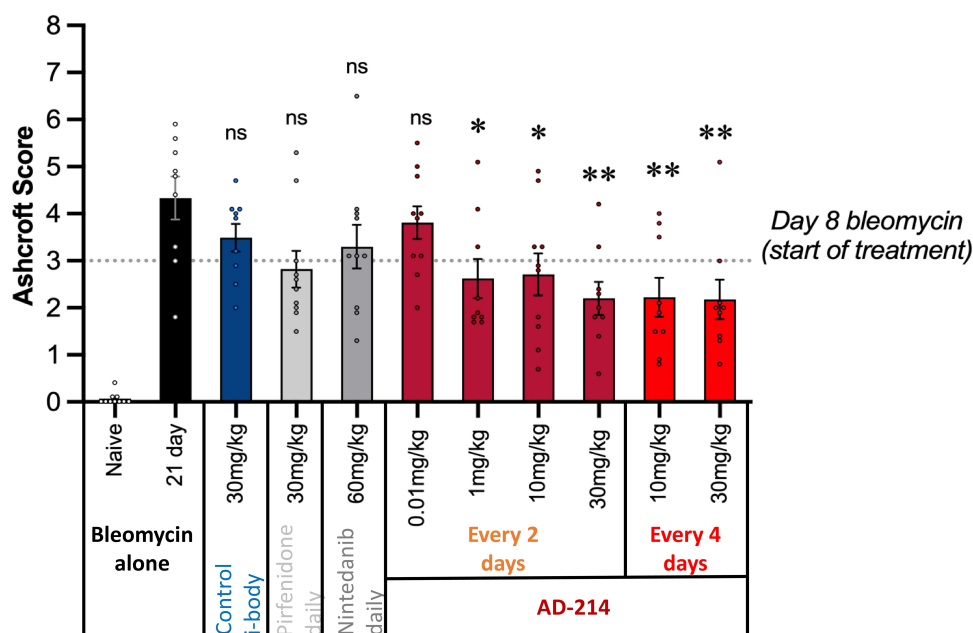
Figure 6. Effect of AD-214 in a bleomycin model of lung fibrosis. The effect of 0.01 to 30 mg/kg AD-214 to abrogate bleomycin-induced lung fibrosis in C57BL/6 mice (15/group) was measured by histology (Masson's trichrome staining and modified Ashcroft scoring). Mice were treated with drug or control as per the dosing schedule detailed in the figure. Horizontal line denotes average Ashcroft score at day 8 post-bleomycin, start of drug treatment. Statistical significance assessed by ANOVA with post hoc Dunnett's comparison test comparing to group 2 (21-day bleomycin and vehicle alone). A difference was considered statistically significant with $p \leq 0.05$. NS not significant. $*p < 0.05$, $**p < 0.01$.

(Figure S8a), as expected. We then confirmed that these T cells could be enriched using immunomagnetic (negative) sorting (live CD3+ T cells >86% of total, Figures S7b and S8b), express CXCR4 as measured by anti-CXCR4 antibody (clone 12G5) staining (Figures S7c and S8a), and were capable of migration *ex vivo* in response to CXCL12 stimulus (Figure S7d). Next, we confirmed that AD-214 has high affinity for CXCR4 in three different T cell donors (K_D: 365.3 ± 161.1 pM; Figure 7a) and in one donor qualified an RO assay method using an anti-CXCR4 antibody clone 12G5 that competes with AD-214 (Figure 7b). As shown in Figure 7b, pre-incubation of AD-214 limits binding of a saturating concentration of 12G5 in a dose-dependent manner (Figure 7b, top panel) from which RO could be calculated (Figure 7b, bottom panel). Lastly, we confirmed that AD-214 inhibited CXCL12-induced migration of T cells in a dose-dependent manner (IC50: 99.9 pM; Figure 7c and Figure S7d), whereas control i-body 21H5-Fc (DAPA) was not inhibitory (Figure S7e). Using these established RO and migration assay conditions, we next sought to link AD-214 occupancy of CXCR4 with efficacy. RO and subsequent migration assays were performed in three different donors. As expected, AD-214 dose-dependently inhibited CXCL12-induced migration of T cells from each donor (Figure 7d). Maximal inhibition was achieved with 57–85% RO, equivalent to 0.7–1 nM of AD-214. The IC_{50} was 11–37% RO, equivalent to 0.07–0.15 nM of AD-214.

Discussion

This report describes the development and characterization of AD-214, an Fc-tagged version of the anti-CXCR4 i-body AD-114 designed to improve the half-life, affinity, and manufacturability of the molecule. AD-114 was selected as it binds specifically to CXCR4 with low nM affinity and displayed anti-fibrotic properties in a bleomycin model of IPF.[19]

In a subsequent study, we explored half-life extension strategies, including fusion of AD-114 to the intrinsically unstructured PAS polypeptide sequence comprising 600 amino acids at its C-terminus (AD-114-PAS), but the affinity of AD-114-PAS for CXCR4 remained modest (low nM).[19] Therefore, as reported here, we elected to fuse AD-114 to an Fc domain to extend the half-life and increase affinity/avidity as well as manufacturability. Indeed, AD-214 binds specifically to CXCR4 with ~ 1,000-fold enhanced affinity compared to the untagged AD-114, consistent with an increased avidity due to the i-body existing as a dimer with a molecular weight of ~75 kDa. Notably, AD-214 bound to FcRn with the same affinity as that reported for other monoclonal antibodies,[20,32] demonstrating that the Fc of AD-214 retains its ability to bind to FcRn, which contributes to prolonged serum half-life of IgGs and Fc-fusion proteins. Moreover, the addition of the DAPA-mutated Fc resulted in a half-life of AD-214 of 22–29 h in non-human primates, as compared to AD-114 which is rapidly cleared.[19] We also show that AD-214 binding to CXCR4 can modulate intracellular signaling resulting from stimulation of this cytokine receptor by the ligand CXCL12, demonstrating that AD-214 is a CXCR4 antagonist inhibiting CXCL12/CXCR4-related signaling pathways.

Importantly, modification of the i-body with the addition of the Fc fusion at the C-terminus maintained the general mechanistic profile to the non-Fc-tagged i-body, AD-114. No change was observed to the CXCR4 binding region of the i-body, inhibition of receptor activation, and subsequent functional effects. In fact, in a dimeric format, these activities are improved, suggesting that the differences in potency are directly due to the improved design of the i-body. The further development of this Fc fusion domain to include two-point DAPA mutations abolishes interactions with Fcγ receptors that mediate effector functions and any Fcγ-mediated
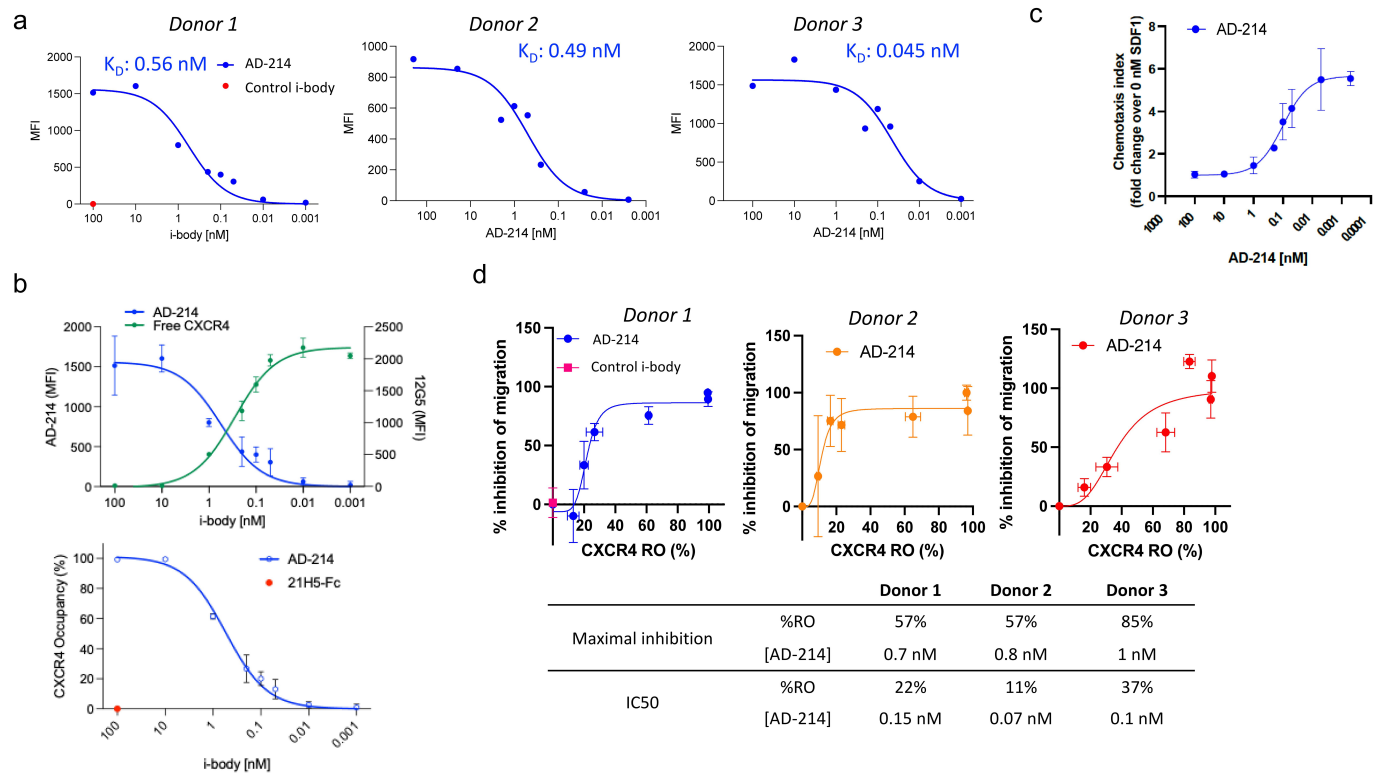
Figure 7. Linking receptor occupancy (RO) with efficacy for AD-214. (a) Binding of AD-214 to CXCR4 on primary human T cells. CD3+ T cells isolated from buffy coats of healthy volunteers were treated with a concentration gradient of AD-214 for 15 min at 37 °C, washed and AD-214 was detected using AF647-conjugated anti-H+L secondary antibody. Data was normalized to background fluorescence minus one (FMO) control and a non-linear regression curve from which the K_D was calculated. Data for three independent donors with n = 2–3 technical replicates per AD-214 concentration is shown. (b) RO assay for AD-214 on primary human T cells. To measure free and occupied CXCR4, the assay was performed as in (a) with the modification that cells were also stained with anti-CXCR4 (clone 12G5)-BrilliantViolet421 antibody which competes with AD-214. Data from a single donor with n = 3 technical replicates per AD-214 concentration is shown. (c) Effect of AD-214 on migration of primary human T cells. Cells were treated with AD-214 as in (a) before being loaded into transwell plates and migration into the bottom chamber in response to SDF-1 (10 nM) quantified 2.5 h later. Data from a single donor with n = 3 technical replicates per AD-214 concentration is shown. (d) Effect of RO on SDF-1 induced T cell migration. Cells were treated with a concentration gradient of AD-214 or control (vehicle diluent) and stained for AD-214 and free CXCR4 as above before being loaded into being loaded into transwell plates and SDF-1 induced migration into the bottom chamber quantified 2.5 h later. Bottom panel shows levels of RO and concentrations of AD-214 required to achieve them. Data were fitted to a non-linear regression analysis from which the IC50 was calculated. Data from 3 donors with n = 3 technical replicates per AD-214 concentration is shown. MFI, median fluorescence intensity. Error bars represent the standard deviation.

destruction of CXCR4-containing hemopoietic cells.[21] The lack of effector functions, specifically ADCC, ADCP, and CDC, was confirmed by *in vitro* cell reporter assays. Thus, when used in a chronic disease setting, there should be no effector-mediated killing of bystander CXCR4-expressing cells necessary for normal physiological function.

Blocking CXCR4 has been shown to inhibit the progression of fibrosis in several preclinical models.[12,33,34] We previously demonstrated that the antifibrotic effects of AD-214 in the unilateral ureteral obstruction (UUO) model of kidney fibrosis[33] and the non-Fc-tagged i-body AD-114 displayed therapeutic efficacy in the bleomycin model, as well as the folic acid model of kidney fibrosis.[13,33] Here, we demonstrate that AD-214 is efficacious when administered therapeutically, 8 days post-bleomycin administration, in the mouse bleomycin model of lung fibrosis. To extend these findings to a human fibrosis model, we used human PCLS treated with a pro-fibrotic cocktail, where AD-214 was antifibrotic, reducing collagen deposition. Interestingly, in both models AD-214 performed better than the standard of care drugs for IPF, pirfenidone (not tested in the PCLS model) and nintedanib, suggesting that AD-214-mediated blockade of CXCR4 may have

superior therapeutic effects. A limitation of the PCLS studies is that we did not explore more translationally relevant doses of AD-214 and nintedanib. The 1 μM dose used in the current study is ~10× higher than the Cmax for nintedanib (standard 150 mg oral dose achieves 37–74 nM), versus 2× lower than the Cmax for AD-214 at a clinically viable IV dose (10 mg/kg). This difference would be further amplified if total exposure is considered. The half-life is 9–12 h for nintedanib and ~48 h for AD-214. Thus, we would hypothesize that titration of AD-214 and nintedanib to concentrations reflecting their in vivo PK, AD-214 would be more efficacious in the PCLS assay, and the same would be true for the bleomycin model where 60 mg/kg daily nintedanib only showed a trend for efficacy, whereas 10–30 mg/kg of AD-214 every 2 to 4 days led to a statistically significant reduction in lung fibrosis.

We focused herein on providing preclinical proof-of-concept for AD-214 as a therapeutic for IPF; however, it is noteworthy that all forms of ILD can cause irreversible pulmonary fibrosis[1] and increased CXCR4 expression has been linked with nonspecific interstitial pneumonia, hypersensitivity pneumonitis, and connective tissue disease-associated ILD,[7] suggesting AD-214 could offer clinical benefit for these

patients. Likewise, AD-214 may be applicable in the treatment of long COVID-19, which has been associated with the accumulation of CXCR4-expressing T cells[35,36] and pulmonary fibrosis,[37] as well as chronic obstructive pulmonary disease, where CXCR4 blockade has been shown to improve lung function.[38]

CXCL12/CXCR4 signaling has been implicated in cellular and molecular processes relevant to IPF that are thought to occur through three key pathways: 1) promoting inflammatory cell and fibrocyte recruitment into the damaged lung tissue;[13,39] 2) promoting secretion of profibrotic factors and epithelial to mesenchymal transition[8,13,33,40,41]; and 3) promoting fibroblast migration and differentiation and ECM deposition during tissue remodeling.[8,13,33] Together with our previous work,[13,33] we have demonstrated that AD-214 (and its analogue, AD-114) can act via all three putative modes of action in a dose-dependent and fibrosis-specific manner.

Inhibition of immune and inflammatory cell recruitment

AD-114 inhibits fibrocyte recruitment to the lungs in the bleomycin model and macrophage infiltration in the folic acid model of kidney fibrosis, and AD-214 inhibits infiltration of macrophages, T cells, and myeloid cells in the UUO model of kidney fibrosis.[33] Consistent with these findings, in the current study we found that AD-214 potently (low pM IC_{50}) inhibits the migration of primary human T cells in response to SDF-1. Though the role of T cells in IPF is controversial, we suggest that they are a useful surrogate for CXCR4+ immune and inflammatory cells, and that AD-214 would inhibit other immune and inflammatory cells involved in IPF, as has been shown for AD-214 and AD-114 in the context of kidney fibrosis and AD-114 in IPF.

Inhibition of secretion of profibrotic factors, proinflammatory factors, and EMT

AD-114 attenuates the production of profibrotic factors and pathways upstream of EMT in renal proximal tubule epithelial cells.[33] In the study reported here, the protein biomarker readouts from the AD-214-treated co-cultures (BioMAP® Fibrosis Panel) revealed a decrease in E-cadherin, an epithelial, but not myofibroblast-expressed, cell adhesion molecule, in the small airway epithelial and myofibroblast co-culture and an increase in the renal epithelial and myofibroblast co-culture, suggesting that AD-214 may have differential effects in these two systems. When epithelial cells undergo EMT, N-cadherin typically increases,[42,43] but there was no effect of AD-214 on N-cadherin expression in either co-culture system. Thus, there appears to be no significant effect of AD-214 on EMT, at least in these models of fibrosis. On the other hand, AD-214 reduced E-cadherin in the small airway epithelial and myofibroblast system and it has been reported that soluble E-cadherin participates in bleomycin-induced pulmonary fibrosis by promoting EMT and the migration of lung fibroblasts.[44] The BioMAP® Fibrosis Panel also revealed that AD-214 conferred a reduction in the inflammatory markers IL-6 and IL-8, suggesting an anti-inflammatory effect of AD-214. Importantly, AD-214 had

a larger impact on fibrosis-related biomarkers in co-cultures of epithelial cells and fibroblasts than on fibroblasts cultured alone, suggesting impacts on cell–cell communication and/or paracrine signaling. Interestingly, there is compelling evidence that the markers that were reduced by AD-214 are all involved in progressing fibrosis. Papiris et al. demonstrated that high levels of IL-6 and IL-8 correlated with acute exacerbations in early IPF and that an increase in IL-6 and IL-8 levels is associated with negative patient outcomes.[45] Additionally, we observed that AD-214 attenuated the expression of MCP-1/CCL2, another chemokine known to play a key role in the pathogenesis of IPF.[46] This is notable because of the potential for redundancy among chemokines involved in the pathogenesis of IPF and suggests that AD-214 offers the unique modality of dual-chemokine pathway inhibition: direct CXCR4 blockade and inhibition of MCP-1/CCL2 expression.

Inhibiting myofibroblast activity, fibroblast migration, and ECM deposition during tissue remodelling

Our previous work has shown that AD-214's antifibrotic effects occur via attenuation of collagen and fibronectin formation in the UUO model, with a similar mechanism observed for AD-114 in the bleomycin model of lung fibrosis.[33] In the present study, screening of AD-214 in the BioMAP® Fibrosis Panel revealed that AD-214 induced robust reduction in expression of Collagen III, one of the major collagens that is increased in lung fibrosis.[44] Similarly, in the PCLS system AD-214 significantly inhibited the deposition of collagen induced by a pro-fibrotic cocktail. A limitation of our study is that we did not evaluate the effects of AD-214 in PCLS isolated from IPF patients, arguably a more disease-relevant model. Interestingly, in a similar study to ours that compared the effect of saracatinib, a small-molecule src kinase inhibitor, the authors found only 2 of 60 genes affected were unique to IPF PCLS compared to healthy control PCLS treated with a fibrotic cocktail, suggesting the fibrotic cocktail-treated PCLS serves as reasonable surrogate for IPF.[47]

Here, we were able to clearly differentiate the mechanism of action of AD-214 from pirfenidone and nintedanib, the two currently approved therapies for IPF. Both nintedanib and pirfenidone were approved based on Phase 3 studies indicating approximately 50% fewer patients who received the drugs suffered an absolute decline of 10% or more in lung function as measured by forced vital capacity;[48–50] however, despite many studies, the precise mechanism of action of these drugs remains uncertain.[51,52] An overlay of the cellular responses to AD-214 compared to each of these drugs has shown that there is little overlap (Figure S5). Thus, AD-214 is a novel antifibrotic with a mechanism of action that does not overlap with the currently approved drugs for IPF. Notably, pirfenidone has been shown to induce an increase in CXCR4 levels,[9] therefore AD-214 may offer added therapeutic benefit when used in combination.

Pharmacological characterization of AD-214 suggests that the anti-fibrotic effects could be contributed by its modulation/blockade of CXCR4-mediated β-arrestin

(IC50: 7 nM)/cAMP (IC50: 7.3 nM) signaling more so than Ca2+ signaling where the IC50 is more modest (56 nM). While we cannot rule out this possibility, epitope mapping studies for AD-114 and two i-bodies with similar affinities for CXCR4 demonstrate distinct epitopes are engaged, leading to different pharmacological outcomes for each i-body,[18] and in follow-up studies only AD-114 and AD-214 have demonstrated significant anti-fibrotic activity.[13,18,19,33] Collectively, these data suggest that the cumulative effect of β-arrestin, cAMP, and Ca2+ signaling pathways downstream of CXCR4 contributes to the overall potency and efficacy of AD-214; however, it would be interesting for future studies to explore the relative contribution of these pathways to the anti-fibrotic effects of AD-214, particularly given the important role of Ca2+ signaling in lung fibrosis identified by others.[53,54]

Lastly, we developed a method to link AD-214 engagement with CXCR4, RO, and efficacy to estimate doses of AD-214 that could be efficacious in future Phase 2 clinical trials. Unpublished results from a Phase 1 clinical trial of AD-214 (NCT04415671) revealed high and durable CXCR4 RO on circulating T cells. Using the RO and migration assay developed herein, we found that 60–85% RO by AD-214 is sufficient to fully inhibit T cell migration, demonstrating that AD-214 does not need to saturate cell surface CXCR4 to inhibit this fibrotic mechanism. Moreover, in the present study, marked inhibition of T cell migration was achieved at far lower RO, 10–40%, suggesting that maximal RO is not necessary for the anti-fibrotic effects mediated by AD-214. Notably, a concentration of 1 nM AD-214 was sufficient to completely inhibit T cell migration and at 0.1 nM achieved 50% inhibition of migration. This is important because 1 nM of AD-214 was found to be the serum concentration after 72 h following a 10 mg/kg IV infusion in the Phase 1 clinical study. When extrapolated to the extended RO levels achieved in the Phase 1 trials for AD-214, these data are supportive of dosing 10–20 mg/kg weekly or every second week via IV administration. However, future studies should develop a PK/pharmacodynamics model for AD-214 and utilize the thresholds of RO required to inhibit T cell migration, to better inform potentially efficacious dosing regimens.

Taken together with the promising safety results from two Phase 1 studies (NCT04415671, NCT05914909), the work herein provides further characterization of the mechanism of action of AD-214 as a potent antifibrotic and anti-inflammatory in models of IPF and demonstrates a promising safety and efficacy of profile. Therefore, further clinical testing is warranted for AD-214 in patients with IPF.

Materials and methods

Study approval

The murine bleomycin experiments were conducted according to MuriGenics' Institutional Animal Care and Use Committee protocol and approved by MuriGenics' Institutional Animal Care and Use Committee (IACUC). In vivo non-human primate PK studies were conducted at ITR Laboratories Canada Inc. in accordance with the principles outlined in the "Guide to the Care and Use of Experimental Animals" as published by the Canadian Council on Animal Care and the NIH's "Guide for the Care and Use of Laboratory Animals" and were approved by the Animal Care Committee of ITR Laboratories Canada Inc. Animal Care Committee acceptance of the study plans was maintained on file at ITR Laboratories Canada Inc. All methods using animals were carried out in accordance with the relevant guidelines and regulations and in accordance with ARRIVE guidelines.[55] Ethical approval for the human buffy coats was granted by the Human Ethics Committee of La Trobe University and the Australian Red Cross Blood Service Ethics Committee and met the requirements of the Australian National Statement on Ethical Conduct in Human Research.

Antibodies and dyes

Sequences of human Fc region-tagged i-bodies were designed and cloned into a pcDNA3.1 vector (GenScript, Singapore). Constructs were transfected into the ExpiCHO (Invitrogen, USA) expression system following the manufacturer's protocol. Fc-tagged i-bodies were purified using orthogonal chromatography steps. Proteins were captured using affinity chromatography (protein A affinity resin, MabSelect PrismA, Cytiva), followed by mixed mode and cation exchange chromatography steps (Capto Adhere ImpRes, Capto S ImpAct, Cytiva, respectively), and buffer exchanged to Formulation Buffer (20 mm sodium succinate, 75 mm arginine, 125 mm sorbitol, pH 4.4) and concentrated to ~20 mg/mL using AKTA Flux S tangential flow filtration system (Cytiva). Polysorbate 20 was added to 0.02% final concentration (w/w) and protein was filtered through a 0.22 μm filter. The following anti-human antibodies were used for flow cytometry: CD3-PE (52127, BD), CD4-V450 (50346, BD), CD8-FITC (51947, BD), CD19-PE-Cy7 (29941, BD), CD14-BrilliantViolet650 (31836, Biolegend), anti-Fc-FITC (309-096-008, AffiniPure F(ab')₂ Fragment Rabbit Anti-Human IgG, Fcγ fragment specific, Jackson ImmunoResearch), anti-human H+L-AF647 (A-21445, Goat anti-Human IgG (H+L) Cross-Adsorbed Secondary Antibody, Alexa Fluor™ 647, Invitrogen). A viability dye live/dead aqua (AF405 Invitrogen) was used to exclude dead cells.

SDS-PAGE

Protein samples (1 μg) were formulated in 4× loading buffer (reducing or non-reducing) and analyzed by SDS-PAGE using 4–15% Bio-Rad® TGX™ gel, Bio-Rad® Precision Plus Protein™ markers, Thermo Fisher Scientific SYPRO® Orange Protein Gel Stain.

Analytical size exclusion chromatography

AD-214 was analyzed on an Agilent LC 1260 Infinity II System outfitted with 1260 Infinity II Vialsampler, 1260 Fraction Collector analytical scale, and 1260 Infinity II Diode Array Detector HS using a TOSOH TSKgel G2000SWxI (7.8 ×

300 mm) column, flowrate 0.5 mL/min, 280 nm BW 4 nm UV detection as follows. 20 mm sodium phosphate, 500 mm NaCl, 250 mm L-Arginine, pH-7.3 ± 0.1 was used as mobile phase buffer and the column was equilibrated for 30 min before initiating the sequence. Samples were adjusted to a concentration of 2.0 mg/mL using mobile phase buffer and 15 μL of diluted AD-214 injected to achieve a 30 μg load per injection. The injection sequence included blank injections, a gel filtration standard injection, and injections of the reference material. Chromatograms were overlayed using Agilent OpenLAB CDS (ChemStation edition) software.

SPR experiments

All SPR experiments were carried out using a BIAcore T200 (Cytiva) instrument.

AD-214 binding to CXCR4 lipoparticles was performed as follows. Streptavidin was immobilized on flow-cell 1 & 2 (Fc1, 2) of Series S CM5 sensor chip using standard amine coupling method at 37°C. Briefly, CM-dextran matrix was activated with 0.2 M 1-ethyl-3-(3-diethylaminopropyl)-carbodiimide hydrochloride (EDC) and 0.05 M N-hydroxy succinimide (NHS) over 300 s, streptavidin (100 μg/mL in 10 mm sodium acetate, pH-4.5) was then passed over the activated surface at a rate of 10 μL/min for 1400 s. Finally, 1 M ethanolamine-HCl (pH 8.5) was injected into both target and reference flow cells for 420 s to deactivate any remaining activated carboxyl groups on the surface. 1×137 mm NaCl, 2.7 mm KCl, 10 mm Na_2HPO_4, and 1.8 mm KH_2PO_4 were used as the immobilization buffer.

A biotin capture strategy was used to immobilize CXCR4 lipoparticles. Biotinylated CXCR4 lipoparticles were diluted 20-fold in 1× running buffer (10 mm HEPES, 150 mm NaCl, 1 mg/mL bovine serum albumin (BSA), pH-7.4) and captured on the active flow cell (Fc2) using a flowrate of 2.0 μL/min and contact time of 3800 s. Fc1 was used as a reference for any nonspecific binding of analyte and the flow cell temperature was set to 25°C.

Single cycle kinetic experiments for AD-214 binding to CXCR4 were performed at 25°C. AD-214 was diluted in 1× running buffer (10 mm HEPES, 150 mm NaCl, 1 mg/mL BSA, pH 7.4) to achieve a concentration series of 20 nM, 6.667 nM, 2.222 nM, 0.7407 nM, and 0.2469 nM and injected over both Fc at a flowrate of 30 μL/min. The contact time was 200 s and dissociation time was 3000 s. Surface was regenerated using 1 mm phosphoric acid for 10 s at a flowrate of 30 μL/min. Data were processed using Biacore S200 Evaluation Software Version 1.0 and fit to a 1:1 binding kinetic model.

A multi-cycle kinetic (MCK) assay was performed to evaluate AD-214 binding to FcRn. AD-214 was immobilized on a CM5 chip using abovementioned standard amine coupling at 25°C. A 1:1 ratio of EDC and NHS was injected for 90 s at a flowrate of 10 μL/min, flowed by 10 μg/mL AD-214 for 20 s and finally 1 M ethanolamine-HCl pH 8.5 was injected for 420 s. Fc1 was used for blank immobilization (reference flow-cell) and 10 mm Na2HPO4/NaH2PO4, 150 mm NaCl, 0.05% Tween-20, pH 5.8 was used as running buffer. Hu FcRn was diluted in 1× running buffer to achieve a concentration series of 250 nM, 125 nM, 62.5 nM, 31.25 nM, 15.625 nM, 7.8125

nM, 3.90625 nM, and 1.93125 nM. Diluted Hu FcRn was flown over immobilized AD-214 using a flowrate of 30 μL/min, 200 s contact time and 300 s dissociation time, temperature 24°C. Surface was regenerated using four 30 s injection of running buffer at a flowrate of 30 μL/min. Data were double referenced against blank injections of buffer (FC2-FC1) and fitted to 1:1 binding kinetic model using Biacore S200 Evaluation Software Version 1.0. Data were fit to a steady-state affinity model using averaging with a 5 s window 4 s before the end of injection.

Membrane protein array

A membrane protein array was performed to profile the specificity of AD-214 for hCXCR4 (Integral Molecular). To determine the optimal antibody concentration and minimize background reactivity, different concentrations of the AD-214 were tested on HEK 293T or QT6 cells expressing either a membrane-bound protein A construct or vector alone (pUC). These tests were conducted in a 384-well format using a single dilution of secondary and tertiary antibodies (Figure S9a-b). Data from assay setup experiments were used to determine the optimal screening conditions for high throughput immunodetection (Figure S9c). Optimal screening concentrations are determined by the background signal (mean fluorescence intensity (MFI)) and false-positive rate in the vector control.

To identify AD-214 binding targets, 5300 different membrane proteins were each expressed in individual wells of HEK-293T cells arrayed in 384-well plates. The cells were then matrixed by pooling individual columns and rows of each 384-well plate. Targets were then identified by detecting antibody binding (using previously optimized conditions described above and summarized in Figure S9c) to overlapping column and row pools, thereby allowing specific deconvolution. Each individual membrane protein target was assigned values corresponding to the binding values of their unique row and column pools. The resulting paired binding values were subsequently normalized and transformed to give a single numerical value for binding of AD-214 against each target protein (Normalized Target Binding). Non-specific fluorescence was determined to be any value below 3 standard deviations of the mean background value.

Pharmacological assays

PathHunter® ß-arrestin, HitHunter® cAMP, PathHunter® Activated GPCR Internalization Assays and Calcium Flux LeadHunter assays (all DiscoveRx) were performed according to the manufacturer's protocol in CXCR4 expressing cells and as described previously.[18]

ADCC and ADCP assays

An ADCC assay was performed using Ramos cells expressing CD20 and CXCR4 as target cells. Reporter cell lines stably expressing human FcγRIIa V158 (high affinity) variant were used as effector cells. A fixed effector to target ratio of 5:1 was used. As a positive control for this assay,

Rituxan (anti-CD20, Biogen) and Darzalex (anti-CD38, Johnson & Johnson) were used. All test antibodies including AD-214 test proteins were evaluated at a top concentration of 100 μg/mL. A log dilution series in triplicate was performed for all antibodies and incubations were performed for 6 h at 37°C with 5% CO_2. After culture, Bio-Glo was added to wells and examined on PerkinElmer 2300 EnSpire Multimode Reader plate reader. Relative light unit (RLU) values were plotted on an XY chart, graphing RLU against log of the antibody concentration, and the data fit to a non-linear regression curve from which the EC_{50} was calculated. Fold induction was calculated by comparing average RLU values to medium only.

For ADCP, the assay was performed as described above, except FcγRIIa (high affinity histidine at amino acid 131) expressing Jurkat Reporter cells were used as effector cells.

CDC assay

The ability of AD-214 to elicit CDC of CXCR4 expressing cells was examined on the Ramos cell line (ATCC, Catalog #CRL-1596). Ramos cells also express CD20. Ramos cells were cultured in log-phase 1n RPMI-1640 Medium (ATCC, Catalog #30–2001) supplemented with 10% fetal calf serum (FCS), 2 mm L-glutamine, 100 IU/mL penicillin, 100 μg/mL streptomycin, 1 mm sodium pyruvate (all from ThermoFisher) with viability >85% as determined automated cell counter (Countess II FL Automated Cell Counter; ThermoFisher; Catalog #AMQAF1000) prior to experiments. Normal human serum complement was purchased from Quidel Corporation, Cat# A113. Fifty thousand target cells were plated on 96-well round bottom tissue culture-treated plates (Corning, Catalog #33077). Twenty-five microliters of antibodies (Rituximab, Darzalex, and AD-214 test proteins) from a top concentration of 100 μg/mL for 7 points (0.1, 1.0, 10, 100, 1,000, 10000, and 100,000 ng/mL) were added in triplicate and incubated for 30 min. Twenty-five microliters of human complement was added for final 25% concentration. The plate was incubated for 3 h at 37°C, 5% CO_2.

Following in-vitro cell culture and test article treatment, cells were harvested and transferred to a 96-well round bottom plate. Plates were centrifuged at 1200 RPM for 5 min at room temperature (RT). Supernatant was aspirated off. Cells were resuspended in 50 μL of 1× PBS with propidium iodide (PI) at a final concentration of 5 μg/mL. Cells were examined by flow cytometry using a BD Biosciences FACSCalibur flow cytometer (San Jose, CA) by using a live gate based on forward vs side scatter parameters. Three thousand total live cell events were collected and examined by histogram for the fluorochrome of interest. The MFI at each antibody concentration was determined by FlowJo analysis software (Ashland, Oregon).

To generate EC_{50} values, total cells were examined by flow cytometry during sample acquisition. Percentage of PI-positive cells was plotted on an XY chart, graphing percentage PI against the log of the concentration, and the data fit

to a non-linear regression curve from which the EC_{50} was calculated.

Pharmacokinetic study in NHPs

Cynomolgus monkeys (*Macaca fascicularis*, Worldwide Primates Inc.) were housed individually in a temperature, humidity, and light-controlled environment (12 h light/dark cycle) throughout the study. No inclusion and exclusion criteria were used. Doses of 0 (vehicle control), 10, 30, or 100 mg/kg of AD-214 were injected intravenously on Days 1, 4, 8, 11, 15, 18, 22, and 25 over a period of 15 min as shown in Table S1. Blood samples were collected from each monkey at the following time points: Day 1: pre-dose, and 15 min, 1, 2, 4, 8, 12, 24, 48, and 72 h post-start of infusion (the 72-h sample was collected prior to Day 4 dosing) and Day 25: pre-dose, and 15 min, 1, 2, 4, 8, 12, 24, 48, and 72 h post-start of infusion. Non-compartmental analysis was obtained from Day 1 and 25 data. Blood samples (1.5 mL) were taken via brachial venipuncture using K2-EDTA as anti-coagulant, centrifuged at 4°C and the resulting plasma was stored at −80°C in Protein LoBind tubes (Eppendorf #0108116). Serum samples were thawed and AD-214 quantified using an ELISA as described previously.[19] Animals were monitored for any signs of overt toxicity through cage-side monitoring for health and behavioral changes.

Transfection of TRex-CHO cell line

TRex-CHO cells were seeded into a 6-well plate in DMEM/F12 media 10% FBS, 10 μg/ml of blasticidin at 37℃ 5% CO_2 and transfected when the culture reached ~60% confluency by adding Fugene HD (Promega) following product recommended volume, followed by a 15-min incubation at RT. After incubation was completed, a mix of Flp-recombinase expression vector POG44 (ThermoFisher, V6005–20) and pcDNA5FRT/TO-hCXCR4 (GenScript) was added following product instructions, and cells were incubated for 24 h at 37℃ 5% CO_2. Media were carefully removed and replaced with DMEM/F-12 10% FBS, 10 μg/ml blasticidin, and 500 μg/ml hygromycin. Media were replaced every 24 h for 3 days and then every 48 h until control cells died, or the transfected cells become over confluent, then cells were subcultured into T75 cm² flasks in α-MEM (Minimum Essential Medium α) containing 10% FBS, 10 μg/ml blasticidin S, 500 μg/ml of hygromycin B.

hCXCR4-CHO cell binding assay

The T-REx™-CHO cell line stably transfected with human CXCR4, hereafter referred to as CHO- hCXCR4, and the parent CHO line were grown in DMEM/F12 1:1 (Gibco) with 10% FCS (SFBS, Bovogen), 1% penicillin/streptomycin (Gibco) and hygromycin B (Gibco, 500 mg/mL). Tetracycline (1 mg/mL) was added to the media for a minimum of 18 h to induce hCXCR4 expression. U266 cells were grown in RPM1 with 10% FCS and 1% penicillin/streptomycin. Cells were cultured in an atmosphere of 5% CO_2 and 95% humidity at 37°C.

Binding of i-bodies to the above cell lines was tested as previously described[33] with modifications. Briefly, cells were seeded 10^5 cells/well into 96-well round bottom tissue culture plates (Corning), washed by centrifugation (1000 × g, 5 min) and resuspension in FACS buffer (2 mm EDTA, 2% FCS, 1× PBS). Cells were then resuspended in FACS buffer containing AD-214 (100–0.002 nM), 21H5-Fc (100–0.125 nM) or vehicle diluent. After incubation for 1 h at 4°C, antibodies were removed and cells were washed twice and blocked using anti-human Fc block (Miltenyi, 130-059-901, 1:50) for 15 min at 4°C followed by staining with Alexa Fluor™ 647-conjugated goat anti-Human IgG (H+L) Cross-Adsorbed Secondary Antibody (Invitrogen, A-21445) or FITC-conjugated F(ab')₂ Fragment Rabbit Anti-Human IgG, Fcγ fragment specific (Jackson ImmunoResearch, 309-096-008).

Primary human T cell isolation

Cryopreserved human buffy coat samples from healthy volunteers (aged >50 years) were provided by the Australian Red Cross Blood Donation Center and prepared as described in Jaffar et al.[7] Briefly, cryopreserved buffy coat samples from individual donors were rapidly thawed in a 37°C water bath and transferred to the media used in downstream migration assays, hereafter referred to as starvation media (RPMI 1640 (15119, Gibco), 1% FCS, 0.1% penicillin/streptomycin), followed by pipetting to resuspend the cells. Unless otherwise status all centrifugation steps were performed at 1,500 rpm for 5 min at 4°C. To lyse red blood cells, the pellet was resuspended in 10× volume of red blood cell lysis buffer (55899, BD Pharm Rad® Lysing Buffer) and incubated for 15 min at RT. White blood cells were washed by pelleting and resuspending in FACS buffer two times and counted by trypan blue exclusion using a hemocytometer. CD3+ T cells were immunomagnetically sorted using the TGX™ Human T Cell Isolation Kit (17951, Stemcell Technologies) following the manufacturer's instructions. Representative dot plots showing CXCR4 expression on CD3 T cells and CD3+ enrichment using the Rad® Human T Cell Isolation Kit in a human buffy coat donor are shown in Figure S8a and Figure S8b, respectively.

RO and subsequent migration assay in primary human T cells

To link RO and migration, 250,000 CD3+ T cells isolated from human buffy coats were incubated with a concentration gradient of i-bodies for 15 min at 37°C. Cells were then seeded into 5.0 μm transwell plates (Rad® HTS Transwell-96 well, CLS3387) and migration monitored in response to SDF-1 (Recombinant Human/Rhesus Macaque/Feline, 350-NS) diluted in starvation media (RPMI/1% FCS) in the bottom chamber. In optimization experiments, we observed that a cell seeding density of 200,000 cells/well and 10 nM of SDF-1α provided an optimal dynamic range for CD3+ T cell migration. In each assay, non-SDF-1α/background migration was determined by including a 0 nM SDF-1 control. After 2.5 h of migration, cells plus media in the bottom well of the transwell were transferred to a V bottom plate, centrifuged, and resuspended in 100 μL of 2% paraformaldehyde (PFA). Ninety

microliters of the cell suspension was acquired on flow cytometer within 2–3 days. Debris were gated out during acquisition. Migration data are expressed as % inhibition of migration where cells treated with SDF-1 alone = maximum and vehicle treated cells = minimum.

Of the cells treated with AD-214, 50000 cells were washed twice, blocked with human Fc block as before and RO was assayed as follows. Cells were incubated for 30 min at 4°C with a cocktail of antibodies that included 1) AF647- or FITC-conjugated anti-human Fc, 2) live/dead aqua, and 3) anti-human CXCR4 12G5-APC (36509) or -BrilliantViolet (BV)421 (36518) (both Biolegend) and CD3-PE (52127, BD). Cells were washed a further two times before being fixed with 4% PFA, washed, and data were acquired for a minimum of 5,000 live cells per sample on a flow cytometer within 24 h. The fluorescence minus one controls (FMO) were used to determine positive staining for AD-214/H+L-AF647 and 12G5-BV421, and for background subtraction. FMO was performed by staining cells with all antibodies/dyes minus the antibody/fluorophore in question. The MFI of the FMO control was subtracted from the respective test conditions to give the true fluorescence of AD-214/H+L-AF657 or Fc-FITC and 12G5-APC or -BV421. Then, RO was calculated as: %RO = 100 × (OCCUPIED/OCCUPIED + FREE), i.e., %RO = 100 × (AD-214 MFI/AD-214 MFI + 12G5 MFI). The RO assay method described herein was developed based upon previous work, as described.[56–60]

BioMAP® assays

The BioMAP® Fibrosis Panel was performed according to the manufacturer's protocol and as described.[61,62] AD-214 was tested in the epithelial cell/myofibroblast co-culture lung (SAEMyoF), renal (REMyoF) systems, and lung fibroblast monoculture (MyoF). Briefly, primary cells pooled from non-diseased multiple donors (n = 3–6) were commercially purchased and handled according to the recommendations of the manufacturers. Early passage (passage 4 or earlier) cells were used to minimize adaptation to cell culture conditions and preserve physiological signaling responses. Adherent cell types were cultured in 96-well plates until confluent. The three systems in the TGX™ Fibrosis Panel were stimulated for 48 h with a cocktail of TNF and TGFβ. AD-214, serially diluted to concentrations of 41, 120, 370, and 1100 nM, was added 1 h before stimulation and remained in the culture. Each plate contained control treatments: positive control (colchicine), negative control (non-stimulated condition), and vehicle diluent control. Soluble factors from supernatants are quantified using either Rad® detection, bead-based multiplex immunoassay or capture ELISA. Direct ELISA was used to measure biomarker levels of cell-associated and cell membrane targets. Effects of AD-214 on cell viability (cytotoxicity) were measured by SRB after 48 h. All test agent and controls were tested at four concentrations, in triplicate. Data acceptance criteria were based on plate performance (% CV of controls) and the performance of positive controls across assays with a comparison to historical controls. Each individual system was confirmed to pass the test of significance of the Pearson's correlation coefficient and 95% of all plates had % CV <20%.

PCLS fibrosis assay

PCLS were supplied by AnaBios (San Diego, USA). Lung tissue was obtained from patients that were tested and confirmed free from major pathogenic viruses and prior history of respiratory disease. Donor demographics are outlined in Table 1. PCLS were 300 μm thick and cryopreserved after preparation, until use in experiments.

Cryopreserved PCLS were thawed for use in experiments and cultured in DMEM with 10% FBS, 1% penicillin-streptomycin for 24 h. After 24 h, media were changed to either control media (DMEM +0.1% FBS) or media with a fibrotic cocktail. Fibrotic cocktail was prepared by the addition of each component and its diluent in parallel to control medium supplemented with 0.1% FBS (GIBCO) as previously published.[63] Fibrotic cocktail consisted of 5 ng/ml recombinant TGF-ß (240-B-002/CF, R&D Systems), 10 ng/mL PDGF-AB (PHG0134, GIBCO), 10 ng/ml TNF (P6804, R&D Systems), and 5 μM LPA (62215, Cayman Chemical) and was replenished at 48 h, with or without treatments. After 48 h, PCLS were treated with fibrotic cocktail containing the addition of either 1 μM AD-214, 1 μM 21H5-DAPA or 1 μM nintedanib (Cayman Chemical), with control PCLS receiving media alone or fibrotic cocktail alone. PCLS were then cultured for additional 72 h before fixation with 4% PFA for histological processing. PCLS were tested in duplicate for each condition.

Sections (5 mm) of fixed PCLS were prepared, stained with hematoxylin and eosin (H&E), Masson's trichrome (Melbourne Histology Platform) and scanned into digital images with a slide-scanner for analysis (Zeiss, Phenomics Australia-Histopathology). Scanned slides stained with Masson trichrome were used to assess degree of fibrosis. Ten non-overlapping fields, with no tissue artifacts or large blood vessels, were analyzed per section. Area of collagen specific stain/total area was assessed using the "Masson trichrome" color deconvolution tool in Image J (image processing program, National Institutes of Health and the Laboratory for Optical and Computational Instrumentation), to give a percent of collagen/total area of interstitial lung tissue. The average of all 10 fields was then calculated to provide a mean percent of collagen/total area per section. For each of the three donors, all available sections were quantified (maximum of $n = 2$, minimum of $n = 1$).

Murine bleomycin model of lung injury

8–10-week-old male C57BL/6 mice were obtained from Envigo Laboratories (Hollister, CA) and assigned 15 mice/group at random. Following arrival, animals were weighed using an electronic balance (Ohaus SCOUT® PRO, Parsippany, NJ), given a clinical examination to ensure that the mice were in good condition and housed at up to 5 per cage. The animals were maintained in ventilated cage racks with HEPA-filtered static cages using sterilized SaniChip bedding 7090A (Harlan Teklad, Hayward, CA). Animal room controls were set to maintain temperature and relative humidity at 20°C ±1°C and 50% ± 20%, respectively. Housing rooms were on a 12:12 light/dark cycle. Animals were provided with ad libitum access to water (via water bottles) and chow (2018 Teklad Global 18% Protein Rodent Diet; Harlan Teklad).

Animals were acclimated on site for at least 3 days before the initiation of dosing and were approximately 8–10 weeks old at the time of BLM instillation.

BLM was purchased from Euroasia as Batch No. 21005 (Bleomycin sulfate from Streptomyces verticillus). BLM was supplied as a dry powder at 1.5 IU per mg and was stored at −80 º pending formulation. The vehicle for BLM (saline) was purchased from Nurse Assist, Inc. (6240 haltom City, TX).

On the day of BLM dosing (Day 0), BLM was dissolved in vehicle (saline) at 0.33 mg/mL. Following anesthetization with an isoflurane/O_2 mixture, 195 mice (plus spares) were administered a single intratracheal (IT) bolus instillation of 100 μL BLM each. This dose corresponded to 0.05 IU/mouse or 2 IU/kg (assuming a body weight of 25 g/mouse). Animals were recovered and then returned to their cages. The remaining 15 mice received no BLM and instead were maintained as naïve controls.

On Day 8, the naïve controls were assigned to Group 1; the BLM-instilled mice were randomized by body weight and assigned to 13 groups of 15 mice each (Groups 2–14). Animals not included in grouping were taken off study. Group-1 animals did not receive any treatment but were maintained on study. Group-3 animals were euthanized on Day 8 and samples were collected as described below. Starting on Day 8, and continuing as indicated through Day 21, animals of Groups 2 and 4–14 were administered control or test articles as follows. Groups 2 and 4–12 were administered by IV injection with (respectively): vehicle (succinate buffer) every other day (Q2D); single doses of AD-214 at 10 or 30 mg/kg; AD-214 at 0.1, 1, 10, or 30 mg/kg, Q2D; 21H5 at with 30 mg/kg, Q2D; or AD-214 at 10 or 30 mg/kg every 4 days (Q4D). Groups 13 and 14 were administered once daily (QD) by oral gavage (PO) with (respectively) 30 mg/kg pirfenidone (Tocris Bioscience) or 60 mg/kg nintedanib. Dosing was repeated at the indicated frequency through Day 20; therefore, the various groups received at total of 7 Q2D doses, 4 Q4D doses, or 13 QD doses. Treatments were administered at dose volumes of 10 mL/kg for PO and 2 mL/kg IV.

On Day 21, one day after the final dose administration (or equivalent time for untreated or single-dose-treated mice; or Day 8 for Group 3), all groups of animals were subjected to terminal cardiocentesis and euthanized by CO_2 narcosis. The left lung from each animal was fixed and processed for staining with Masson's trichrome, and fibrosis was assessed per the modified Ashcroft scale (Table S2).

The left lung was recovered by necropsy and inflated with 10% neutral-buffered formalin (NBF). Each lung was drop-fixed in NBF overnight at RT, then transferred to 70% ethanol and stored at RT. The fixed tissue was processed by standard methodologies, embedded in paraffin, sectioned, and stained with Masson's trichrome. The trichrome-stained sections were used to assess fibrosis via the modified Ashcroft scale[64] (see Supplementary Table S1) for 10 fields per sample under 10× magnification. A first batch of trichrome-stained sections were rejected due to folding of sections leading to false positive Ashcroft Scores (for example, in naïve mice that did not receive bleomycin). A second set of sections were prepared and assessed by a reader (MuriGenics) blinded to the study group (except naïve). These sections also were assessed by an independent reader (Dr Clayton Yates, of Tuskegee University,

Director for the Center for Biomedical Research) to verify the MuriGenics assessment.

Data analysis and software

Flow cytometry data were analyzed using BD FACSDiva™ and FlowJo v10 software. Graphs and statistical analyses were generated using GraphPad Prism v9.

For PCLS assay data, significance was evaluated with one-way ANOVA with Tukey's multiple comparison test.

For BLM model data, one-way ANOVA with post hoc Dunnett's test was performed.

For the NHP PK assay, non-compartmental analysis of AD-214 concentrations in serum data sets obtained on Days 1 and 25 was performed by using the Phoenix® WinNonlin® 6.4 software. The following configuration was used for the analysis: Sampling Method: Rich; AUC Calculation Method: Linear Trapezoidal with Linear Interpolation; Lambda Z Method: Best fit for Lambda z, Log regression; Weighting (Lambda z calculation): Uniform. The extrapolated to infinity ($AUC\infty$) was estimated using the linear trapezoidal rule, by adding together the $AUC_{0-Tlast}$ and the extrapolated area calculated as the ratio of $Clast/\lambda z$, where Clast was the last quantifiable concentration and λz was the terminal rate constant. The half-life ($t_{1/2}$), calculated from λz, was determined by linear regression analysis using at least three quantifiable concentrations in the elimination phase of the concentration time curve (not including Tmax).

For analysis of the BioMAP® data, biomarker measurements were profiled in triplicate for test agent-treated samples and divided by the average of vehicle control samples (at least six vehicle controls from the same plate) to generate a ratio that is then log10 transformed. Significance prediction envelopes were calculated using historical vehicle control data at a 95% confidence interval. Statistical p-values were calculated from unpaired t-tests of raw assay values compared to vehicle controls. Biomarker readouts were designated hits if the values were significantly different from controls ($p < 0.01$), values were outside of the significance envelope (symmetrical upper and lower bound values of historical vehicle controls at a 95% confidence interval), and at least one concentration had an effect size >20% vs vehicle controls.

Disclosure statement

J.P.L, L.O., K.T., L.K., D.J.H., A.T., and C.H are current or previous employees of AdAlta Ltd. M.F. is a consultant for AdAlta Ltd.

ORCID

Jason P. Lynch http://orcid.org/0000-0003-0889-2616
Michael Foley http://orcid.org/0000-0003-1349-4698

Author contributions

J.P.L, L.O., K.T, L.K., C.H., D.H., M.F., and A.T. designed the research. J.P.L, L.O., K.T, L.K., and C.H. performed the research. J.P.L and M.F. wrote the paper. All authors reviewed the results and approved the final version of the manuscript.

Data availability statement

The AD-214 protein sequence is available at Github repository, https://github.com/jpl37/AD-214-sequence/blob/0555cdd297ce3c246b37ddda2afa0704e838df5/README.md.

References

1. Maher TM. Interstitial lung disease: a review. JAMA. 2024;331 (19):1655–1665. doi: 10.1001/jama.2024.3669.
2. Mackintosh JA, Keir G, Troy LK, Holland AE, Grainge C, Chambers DC, Sandford D, Jo HE, Glaspole I, Wilsher M, et al. Treatment of idiopathic pulmonary fibrosis and progressive pulmonary fibrosis: a position statement from the thoracic society of Australia and New Zealand 2023 revision. Respirology. 2024;29 (2):105–135. doi: 10.1111/resp.14656.
3. Oberlin E, Amara A, Bachelerie F, Bessia C, Virelizier J-L, Arenzana-Seisdedos F, Schwartz O, Heard J-M, Clark-Lewis I, Legler DF, et al. The CXC chemokine SDF-1 is the ligand for LESTR/fusin and prevents infection by T-cell-line-adapted HIV-1. Nature. 1996;382(6594):833–835. doi: 10.1038/32833a0.
4. Bleul CC, Farzan M, Choe H, Parolin C, Clark-Lewis I, Sodroski J, Springer TA. The lymphocyte chemoattractant SDF-1 is a ligand for LESTR/fusin and blocks HIV-1 entry. Nature. 1996;382 (6594):829–833. doi: 10.1038/32829a0.
5. Kucia M, Jankowski K, Reca R, Wysoczynski M, Bandura L, Allendorf DJ, Zhang J, Ratajczak J, Ratajczak MZ. CXCR4–SDF-1 signalling, locomotion, chemotaxis and adhesion. J Mol Histol. 2004;35(3):233–245. doi: 10.1023/B:HIJO.0032355.66152.b8.
6. Miller RJ, Banisadr G, Bhattacharyya BJ. CXCR4 signaling in the regulation of stem cell migration and development. J Neuroimmunol. 2008;198(1–2):31–38. doi: 10.1016/j.jneuroim.2008.04.008.
7. Jaffar J, Griffiths K, Oveissi S, Duan M, Foley M, Glaspole I, Symons K, Organ L, Westall G. CXCR4(+) cells are increased in lung tissue of patients with idiopathic pulmonary fibrosis. Respir Res. 2020;21(1):221. doi: 10.1186/s2931-020-01467-0.
8. Li F, Xu X, Geng J, Wan X, Dai H. The autocrine CXCR4/CXCL12 axis contributes to lung fibrosis through modulation of lung fibroblast activity. Exp Ther Med. 2020;19:1844–1854. doi: 10.3892/etm.2020.8433.
9. Derlin T, Jaeger B, Jonigk D, Apel RM, Freise J, Shin H-O, Weiberg D, Warnecke G, Ross TL, Wester H-J, et al. Clinical molecular imaging of pulmonary CXCR4 expression to predict outcome of pirfenidone treatment in idiopathic pulmonary fibrosis. Chest. 2021;159(3):1094–1106. doi: 10.1016/j.chest.2020.08.2043.
10. Sivakumar P, Ammar R, Thompson JR, Luo Y, Streltsov D, Porteous M, McCoubrey C, Cantu E, Beers MF, Jarai G, et al. Integrated plasma proteomics and lung transcriptomics reveal

novel biomarkers in idiopathic pulmonary fibrosis. Respir Res. 2021;22(1):273. doi: 10.1186/s2931-021-01860-3.

11. Watanabe M, Matsuyama W, Shirahama Y, Mitsuyama H, Oonakahara K-I, Noma S, Higashimoto I, Osame M, Arimura K. Dual effect of AMD3100, a CXCR4 antagonist, on bleomycin-induced lung inflammation. The J Immunol. 2007;178 (9):5888–5898. doi: 10.4049/jimmunol.178.9.5888.

12. Song JS, Kang CM, Kang HH, Yoon HK, Kim YK, Kim KH, Moon HS, Park SH. Inhibitory effect of CXC chemokine receptor 4 antagonist AMD3100 on bleomycin induced murine pulmonary fibrosis. Exp Mol Med. 2010;42(6):465–472. doi: 10.3858/emm. 2010.42.6.048.

13. Griffiths K, Habiel DM, Jaffar J, Binder U, Darby WG, Hosking CG, Skerra A, Westall GP, Hogaboam CM, Foley M, et al. Anti-fibrotic effects of CXCR4-targeting i-body AD-114 in preclinical models of pulmonary fibrosis. Sci Rep. 2018;8(1):3212. doi: 10.1038/s1598-018-20811-5.

14. Fouquet G, Guidez S, Richez V, Stoppa A-M, Le Tourneau C, Macro M, Gruchet C, Bobin A, Moya N, Syshenko T, et al. Phase I dose-escalation study of F0067, a humanized anti-CXCR4 mono-clonal antibody alone and in combination with lenalidomide and low-dose dexamethasone, in relapsed or refractory multiple myeloma. Oncotarget. 2018;9(35):23890–23899. doi: 10.18632/oncotarget.25156.

15. Liu SH, Gu Y, Pascual B, Yan Z, Hallin M, Zhang C, Fan C, Wang W, Lam J, Spilker ME, et al. A novel CXCR4 antagonist IgG1 antibody (PF-07143) for the treatment of hematologic malignancies. Blood Adv. 2017;1(15):1088–1100. doi: 10.1182/bloodadvances.2003921.

16. Peng SB, Zhang X, Paul D, Kays LM, Ye M, Vaillancourt P, Dowless M, Stancato LF, Stewart J, Uhlik MT, et al. Inhibition of CXCR4 by LY4587, a fully humanized anti-CXCR4 antibody induces apoptosis of hematological malignancies. PLOS ONE. 2016;11(3):e0585. doi: 10.1371/journal.pone.00585.

17. Kashyap MK, Kumar D, Jones H, Amaya-Chanaga CI, Choi MY, Melo-Cardenas J, Ale-Ali A, Kuhne MR, Sabbatini P, Cohen LJ, et al. Ulocuplumab (BMS-96564/MDX1338): a fully human anti-CXCR4 antibody induces cell death in chronic lymphocytic leukemia mediated through a reactive oxygen species-dependent pathway. Oncotarget. 2016;7(3):2809–2822. doi: 10.18632/oncotarget.6465.

18. Griffiths K, Dolezal O, Cao B, Nilsson SK, See HB, Pfleger KDG, Roche M, Gorry PR, Pow A, Viduka K, et al. I-bodies, human single domain antibodies that antagonize chemokine receptor CXCR4. J Biol Chem. 2016;291(24):12641–12657. doi: 10.1074/jbc.M116.71050.

19. Griffiths K, Binder U, McDowell W, Tommasi R, Frigerio M, Darby WG, Hosking CG, Renaud L, Machacek M, Lloyd P, et al. Half-life extension and non-human primate pharmacokinetic safety studies of i-body AD-114 targeting human CXCR4. Mabsaustin. 2019;11(7):1331–1340. doi: 10.1080/10862.2019.16652.

20. Nath N, Godat B, Flemming R, Urh M. Deciphering the interaction between neonatal fc receptor and antibodies using a homogeneous bioluminescent immunoassay. The J Immunol. 2021;207(4):1211–1221. doi: 10.4049/jimmunol.20181.

21. Di Padova TH, Rondeau JR. Il-17 antagonistic antibodies. US patent. 2014.

22. Houck KA, Dix DJ, Judson RS, Kavlock RJ, Yang J, Berg EL. Profiling bioactivity of the ToxCast chemical library using BioMAP primary human cell systems. J Biomol Screen. 2009;14 (9):1054–1066. doi: 10.1177/1057135525.

23. Kleinstreuer NC, Yang J, Berg EL, Knudsen TB, Richard AM, Martin MT, Reif DM, Judson RS, Polokoff M, Dix DJ, et al. Phenotypic screening of the ToxCast chemical library to classify toxic and therapeutic mechanisms. Nat Biotechnol. 2014;32 (6):583–591. doi: 10.1038/nbt.2914.

24. Lam M, Lamanna E, Organ L, Donovan C, Bourke JE. Perspectives on precision cut lung slices—powerful tools for investigation of mechanisms and therapeutic targets in lung diseases. Front Pharmacol. 2023;14. doi: 10.3389/fphar.2023.12889.

25. John AE, Graves RH, Pun KT, Vitulli G, Forty EJ, Mercer PF, Morrell JL, Barrett JW, Rogers RF, Hafeji M, et al. Translational pharmacology of an inhaled small molecule αvβ6 integrin inhibitor for idiopathic pulmonary fibrosis. Nat Commun. 2020;11 (1):1–14. doi: 10.1038/s1467-020-18397-6.

26. Alsafadi HN, Staab-Weijnitz CA, Lehmann M, Lindner M, Peschel B, Königshoff M, Wagner DE. An ex vivo model to induce early fibrosis-like changes in human precision-cut lung slices. Am J Physiol-Lung Cellular Mol Physiol. 2017;312(6):L896–L902. doi: 10.1152/ajplung.00084.2017.

27. Lehmann M, Buhl L, Alsafadi HN, Klee S, Hermann S, Mutze K, Ota C, Lindner M, Behr J, Hilgendorff A, et al. Differential effects of Nintedanib and Pirfenidone on lung alveolar epithelial cell function in ex vivo murine and human lung tissue cultures of pulmonary fibrosis. Respir Res. 2018;19(1):1–12. doi: 10.1186/s2931-018-0876-y.

28. Mercer PF, Woodcock HV, Eley JD, Platé M, Sulikowski MG, Durrenberger PF, Franklin L, Nanthakumar CB, Man Y, Genovese F, et al. Exploration of a potent PI3 kinase/mTOR inhibitor as a novel anti-fibrotic agent in IPF. Thorax. 2016;71 (8):701–711. doi: 10.1136/thoraxjnl-2015-27429.

29. Lehmann M, Buhl L, Alsafadi HN, Klee S, Hermann S, Mutze K, Ota C, Lindner M, Behr J, Hilgendorff A, et al. Differential effects of Nintedanib and Pirfenidone on lung alveolar epithelial cell function in ex vivo murine and human lung tissue cultures of pulmonary fibrosis. Respir Res. 2018;19(1):175. doi: 10.1186/s2931-018-0876-y.

30. Pakhomova A, Pershina O, Bochkov P, Ermakova N, Pan E, Sandrikina L, Dagil Y, Kogai L, Grimm W-D, Zhukova M, et al. Anti-inflammatory and antifibrotic potential of longidaze in bleomycin-induced pulmonary fibrosis. Life (Basel). 2023;13 (9):1932. doi: 10.3390/life91932.

31. Ishida Y, Kuninaka Y, Mukaida N, Kondo T. Immune mechanisms of pulmonary fibrosis with Bleomycin. Int J Mol Sci. 2023;24 (4):3149. doi: 10.3390/ijms43149.

32. Suzuki T, Ishii-Watabe A, Tada M, Kobayashi T, Kanayasu-Toyoda T, Kawanishi T, Yamaguchi T. Importance of neonatal FcR in regulating the serum half-life of therapeutic proteins containing the Fc domain of human IgG1: a comparative study of the affinity of monoclonal antibodies and Fc-fusion proteins to human neonatal FcR. J Immunol. 2010;184(4):1968–1976. doi: 10.4049/jimmunol.03296.

33. Cao Q, Huang C, Yi H, Gill AJ, Chou A, Foley M, Hosking CG, Lim KK, Triffon CF, Shi Y, et al. A single-domain i-body, AD-114, attenuates renal fibrosis through blockade of CXCR4. JCI Insight. 2022;7(4). doi: 10.1172/jci.insight.13018.

34. Makino H, Aono Y, Azuma M, Kishi M, Yokota Y, Kinoshita K, Takezaki A, Kishi J, Kawano H, Ogawa H, et al. Antifibrotic effects of CXCR4 antagonist in bleomycin-induced pulmonary fibrosis in mice. J Med Invest. 2013;60(1.2):127–137. doi: 10.2152/jmi.60.127.

35. Yin K, Peluso MJ, Luo X, Thomas R, Shin M-G, Neidleman J, Andrew A, Young KC, Ma T, Hoh R, et al. Long COVID manifests with T cell dysregulation, inflammation and an uncoordinated adaptive immune response to SARS-CoV-2. Nat Immunol. 2024;25(2):218–225. doi: 10.1038/s1590-023-01724-6.

36. Neidleman J, Luo X, George AF, McGregor M, Yang J, Yun C, Murray V, Gill G, Greene WC, Vasquez J, et al. Distinctive features of SARS-CoV-2-specific T cells predict recovery from severe COVID-19. Cell Rep. 2021;36(3):19414. doi: 10.1016/j.celrep. 2021.19414.

37. Duong-Quy S, Vo-Pham-Minh T, Tran-Xuan Q, Huynh-Anh T, Vo-Van T, Vu-Tran-Thien Q, Nguyen-Nhu V. Post-COVID-19 pulmonary fibrosis: facts—challenges and futures: a narrative review. Pulm Ther. 2023;9(3):295–307. doi: 10.1007/s1030-023-00226-y.

38. Dupin I. Blocking CXCR4 improves pulmonary and cardiac outcomes in a mouse model of early COPD. Eur Respir J. 2023;62: OA4243. doi: 10.1183/13003.congress-2023.OA4243.

39. Phillips RJ, Burdick MD, Hong K, Lutz MA, Murray LA, Xue YY, Belperio JA, Keane MP, Strieter RM. Circulating fibrocytes traffic

to the lungs in response to CXCL12 and mediate fibrosis. J Clin Invest. 2004;114(3):438–446. doi: 10.1172/JCI420997.

40. Tang H, Xu Y, Zhang Z, Zeng S, Dong W, Jiao W, Hu X. SDF-1/CXCR4 induces epithelial-mesenchymal transition through activation of the Wnt/β-catenin signaling pathway in rat chronic allograft nephropathy. Mol Med Report. 2019;19:3696–3706. doi: 10.3892/mmr.2019.10045.

41. Li XQ, Ma Q, Xu Q, Liu H, Lei J, Duan W, Bhat K, Wang F, Wu E, Wang Z, et al. SDF-1/CXCR4 signaling induces pancreatic cancer cell invasion and epithelial–mesenchymal transition in vitro through non-canonical activation of hedgehog pathway. Cancer Lett. 2012;322(2):169–176. doi: 10.1016/j.canlet.2012.02.035.

42. Zhang X, Liu G, Kang Y, Dong Z, Qian Q, Ma X. N-Cadherin expression is associated with acquisition of EMT phenotype and with enhanced invasion in erlotinib-resistant lung cancer cell lines. PLOS ONE. 2013;8(3):e7692. doi: 10.1371/journal.pone.07692.

43. Lu W, Eapen MS, Hardikar A, Chia C, Robertson I, Singhera GK, Hackett TL, Sohal SS. Epithelial–mesenchymal transition changes in nonsmall cell lung cancer patients with early COPD. Erj Open Res. 2023;9(6):00581–02023. doi: 10.1183/20541.00581-2023.

44. Jessen H, Hoyer N, Prior TS, Frederiksen P, Karsdal MA, Leeming DJ, Bendstrup E, Sand JMB, Shaker SB. Turnover of type I and III collagen predicts progression of idiopathic pulmonary fibrosis. Respir Res. 2021;22(1):205. doi: 10.1186/s2931-021-01801-0.

45. Papiris SA, Tomos IP, Karakatsani A, Spathis A, Korbila I, Analitis A, Kolilekas L, Kagouridis K, Loukides S, Karakitsos P, et al. High levels of IL-6 and IL-8 characterize early-on idiopathic pulmonary fibrosis acute exacerbations. Cytokine. 2018;102:168–172. doi: 10.1016/j.cyto.2017.08.019.

46. Baran CP, Opalek JM, McMaken S, Newland CA, O'Brien JM, Hunter MG, Bringardner BD, Monick MM, Brigstock DR, Stromberg PC, et al. Important roles for macrophage colony-stimulating factor, CC chemokine ligand 2, and mononuclear phagocytes in the pathogenesis of pulmonary fibrosis. Am J Respir Crit Care Med. 2007;176(1):78–89. doi: 10.1164/rccm.20609-1279OC.

47. Ahangari F, Becker C, Foster DG, Chioccioli M, Nelson M, Beke K, Wang X, Justet A, Adams T, Readhead B, et al. Saracatinib, a selective src kinase inhibitor, blocks fibrotic responses in preclinical models of pulmonary fibrosis. Am J Respir Crit Care Med. 2022;206(12):1463–1479. doi: 10.1164/rccm.22010-3832OC.

48. Lederer DJ, Bradford WZ, Fagan EA, Glaspole I, Glassberg MK, Glasscock KF, Kardatzke D, King TE, Lancaster LH, Nathan SD, et al. Sensitivity analyses of the change in FVC in a phase 3 trial of pirfenidone for idiopathic pulmonary fibrosis. Chest. 2015;148(1):196–201. doi: 10.1378/chest.14-2817.

49. King TE Jr., Bradford WZ, Castro-Bernardini S, Fagan EA, Glaspole I, Glassberg MK, Gorina E, Hopkins PM, Kardatzke D, Lancaster L, et al. A phase 3 trial of pirfenidone in patients with idiopathic pulmonary fibrosis. N Engl J Med. 2014;370(22):2083–2092. doi: 10.1056/NEJMoa2582.

50. Flaherty KR, Wells AU, Cottin V, Devaraj A, Walsh SLF, Inoue Y, Richeldi L, Kolb M, Tetzlaff K, Stowasser S, et al. Nintedanib in progressive fibrosing interstitial lung diseases. N Engl J Med. 2019;381(18):1718–1727. doi: 10.1056/NEJMoa8681.

51. Ghumman M, Dhamecha D, Gonsalves A, Fortier L, Sorkhdini P, Zhou Y, Menon JU. Emerging drug delivery strategies for idiopathic pulmonary fibrosis treatment. Eur J Pharm Biopharm. 2021;164:1–12. doi: 10.1016/j.ejpb.2021.03.017.

52. Sartiani L, Bartolucci G, Pallecchi M, Spinelli V, Cerbai E. Pharmacological basis of the antifibrotic effects of pirfenidone: mechanistic insights from cardiac in-vitro and in-vivo models. Front Cardiovasc Med. 2022;9:71499. doi: 10.3389/fcvm.2022.71499.

53. Mukherjee S, Ayaub E, Murphy J, Lu C, Kolb M, Ask K, Janssen L. Disruption of calcium signaling in fibroblasts and attenuation of bleomycin-induced fibrosis by nifedipine. Am J Respir Cell Mol Biol. 2015;53(4):450–458. doi: 10.1165/rcmb.2015-0009OC.

54. Wolffs K, Li R, Mansfield B, Pass DA, Bruce RT, Huang P, de Araújo RP, Haddadi BS, Mur LAJ, Dally J, et al. Calcium-sensing receptor as a novel target for the treatment of idiopathic pulmonary fibrosis. Biomolecules. 2025;15(4):509. doi: 10.3390/biom40509.

55. Kilkenny C, Browne WJ, Cuthill IC, Emerson M, Altman DG. Improving bioscience research reporting: the ARRIVE guidelines for reporting animal research. PLOS Biol. 2010;8(6):e0412. doi: 10.1371/journal.pbio.10412.

56. Schwickart M, Chavez C, Henderson S, Vainshtein I, Standifer N, DelNagro C, Mehrzai F, Schneider A, Roskos L, Liang M, et al. Evaluation of assay interference and interpretation of CXCR4 receptor occupancy results in a preclinical study with MEDI3185, a fully human antibody to CXCR4. Cytometry B Clin Cytom. 2016;90(2):209–219. doi: 10.1002/cyto.b.21327.

57. Crees ZD, Stockerl-Goldstein K, Sorani E, Ickowicz D, Darvish L, DiPersio JF. Prolonged CXCR4 receptor occupancy by motixafortide following a single subcutaneous injection is associated with extended mobilization of CD34+ cells in peripheral blood for > 24 hours. Transplant Cellular Ther. 2024;30(2):S390. doi: 10.1016/j.jtct.2023.12.546.

58. Wang R, Gao C, Raymond M, Dito G, Kabbabe D, Shao X, Hilt E, Sun Y, Pak I, Gutierrez M, et al. An integrative approach to inform optimal administration of OX40 agonist antibodies in patients with advanced solid tumors. Clin Cancer Res. 2019;25(22):6709–6720. doi: 10.1158/1078-0432.CCR-19-0526.

59. Sison EA, Magoon D, Li L, Annesley CE, Rau RE, Small D, Brown P. Plerixafor as a chemosensitizing agent in pediatric acute lymphoblastic leukemia: efficacy and potential mechanisms of resistance to CXCR4 inhibition. Oncotarget. 2014;5(19):8947–8958. doi: 10.18632/oncotarget.2407.

60. Sison EAR, Magoon D, Li L, Annesley CE, Romagnoli B, Douglas GJ, Tuffin G, Zimmermann J, Brown P. POL5551, a novel and potent CXCR4 antagonist, enhances sensitivity to chemotherapy in pediatric ALL. Oncotarget. 2015;6(31):30902–30918. doi: 10.18632/oncotarget.5094.

61. Kunkel EJ, Dea M, Ebens A, Hytopoulos E, Melrose J, Nguyen D, Ota KS, Plavec I, Wang Y, Watson SR, et al. An integrative biology approach for analysis of drug action in models of human vascular inflammation. FASEB J. 2004;18(11):1279–1281. doi: 10.1096/fj.04-1538fje.

62. Kunkel EJ, Plavec I, Nguyen D, Melrose J, Rosler ES, Kao LT, Wang Y, Hytopoulos E, Bishop AC, Bateman R, et al. Rapid structure-activity and selectivity analysis of kinase inhibitors by BioMAP analysis in complex human primary cell-based models. Assay Drug Dev Technol. 2004;2(4):431–441. doi: 10.1089/adt.2004.2.431.

63. Alsafadi HN, Staab-Weijnitz CA, Lehmann M, Lindner M, Peschel B, Königshoff M, Wagner DE. An ex vivo model to induce early fibrosis-like changes in human precision-cut lung slices. Am J Physiol Lung Cell Mol Physiol. 2017;312(6):L896–l902. doi: 10.1152/ajplung.00084.2017.

64. Ashcroft T, Simpson JM, Timbrell V. Simple method of estimating severity of pulmonary fibrosis on a numerical scale. J Clin Pathol. 1988;41(4):467–470. doi: 10.1136/jcp.41.4.467.